NASA TECHNICAL NOTE

NASA TN D-4013

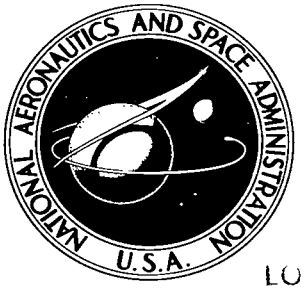

STATIC STABILITY INVESTIGATION OF A SINGLE-STAGE SOUNDING ROCKET AT MACH NUMBERS FROM 0.60 TO 1.20

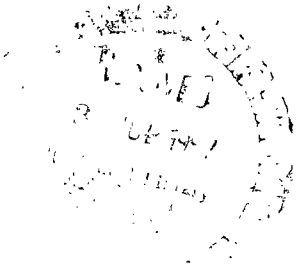

by James C. Ferris

Langley Research Center
Langley Station, Hampton, Va.

NATIONAL AERONAUTICS AND SPACE ADMINISTRATION • WASHINGTON, D. C. • JUNE 1967

STATIC STABILITY INVESTIGATION OF A SINGLE-STAGE SOUNDING ROCKET AT MACH NUMBERS FROM 0.60 TO 1.20

By James C. Ferris

Langley Research Center
Langley Station, Hampton, Va.

NATIONAL AERONAUTICS AND SPACE ADMINISTRATION

For sale by the Clearinghouse for Federal Scientific and Technical Information
Springfield, Virginia 22151 – CFSTI price $3.00

STATIC STABILITY INVESTIGATION OF A SINGLE-STAGE SOUNDING ROCKET AT MACH NUMBERS FROM 0.60 TO 1.20

By James C. Ferris
Langley Research Center

SUMMARY

Tests were conducted on a 1/2-scale model of a single-stage meteorological sounding rocket to determine the effect of body length and fin cant angle on the aerodynamic characteristics of the model. Tests were conducted through an angle-of-attack range from -3° to 21° at fin roll angles of 0°, 22.5°, and 45°. The Mach number was varied from 0.60 to 1.20 with a constant Reynolds number of 9.8×10^6 per meter (3.0×10^6 per foot). Tests were made for two models with fineness ratios of 18.2 and 23.8. Results were obtained with fins off and with fins on at cant angles of 0° and 2°.

The results indicate that the models had similar pitch-up tendencies in the angle-of-attack range from approximately 8° to approximately 16° at all Mach numbers of this investigation. Both models had large yawing moments at the high angles of attack. The canted fins produced positive rolling moments through the angle-of-attack range from -4° to 12° at all Mach numbers, and they improved the longitudinal stability of the short model in the angle-of-attack range from -2° to 2°.

INTRODUCTION

The Arcas meteorological sounding rocket has been used by the National Aeronautics and Space Administration and other government agencies for conducting high-altitude research. This vehicle, a single-stage solid fuel tube launched rocket, has had modifications to improve the reliability and allow the vehicle to be used for more varied missions. In order to meet the requirements for the several versions of the vehicle, it was considered necessary to conduct wind-tunnel investigations to determine the aerodynamic characteristics associated with body length, fins, and fin cant angle.

Reference 1 presents the results of an investigation conducted in the Langley Unitary Plan wind tunnel at Mach numbers from 1.50 to 4.63, at angles of attack from -4° to 20°, at angles of sideslip from -4° to 8°, and at a Reynolds number per meter of about 9.8×10^6 (3.0×10^6 per foot). Two models were investigated. A short model

(fineness ratio of 18.2) was representative of the Arcas Robin meteorological rocket vehicle, whereas a long model (fineness ratio of 23.8) was representative of the Arcas vehicle as modified by NASA to accommodate a bioscience payload. The purpose of this paper is to present the results of an investigation of the same two models conducted in the Langley 8-foot transonic pressure tunnel at Mach numbers from 0.60 to 1.20, at angles of attack from -3° to 21°, at roll angles of 0°, 22.5°, and 45°, and at fin cant angles of 0° and 2°. The Reynolds number was held constant at 9.8×10^6 per meter (3.0×10^6 per foot).

SYMBOLS

The aerodynamic force and moment data are referred to the body-axis system with the moment reference center located at 70 percent of the body length for both the short body and the long body.

C_A axial-force coefficient, $\frac{\text{Axial force}}{qS}$

$C_{A,b}$ base axial-force coefficient, $\frac{\text{Base axial force}}{qS}$

$C_{A,corr}$ axial force corrected for base axial force

C_l rolling-moment coefficient, $\frac{\text{Rolling moment}}{qSd}$

C_m pitching-moment coefficient, $\frac{\text{Pitching moment}}{qSd}$

C_N normal-force coefficient, $\frac{\text{Normal force}}{qS}$

C_n yawing-moment coefficient, $\frac{\text{Yawing moment}}{qSd}$

$C_{p,b}$ base-pressure coefficient, $\frac{p_b - p}{q}$

C_Y side-force coefficient, $\frac{\text{Side force}}{qS}$

d body diameter, centimeters (inches)

M free-stream Mach number

p	free-stream static pressure, newtons per meter^2 (pounds per foot^2)
p_b	static pressure at base of model, newtons per meter^2 (pounds per foot^2)
q	free-stream dynamic pressure, newtons per meter^2 (pounds per foot^2)
S	maximum cross-sectional area of body, meters^2 (feet^2)
x_{cp}	center-of-pressure location, percent body length
α	angle of attack of model center line, degrees
δ_F	fin cant angle (setting with reference to body center line), degrees
ϕ	fin roll angle, positive clockwise as viewed upstream aft of the model, degrees

APPARATUS AND TESTS

The investigation was made in the Langley 8-foot transonic pressure tunnel. The test section of this tunnel is square in cross section with slotted upper and lower walls to permit continuous operation through the transonic speed range. The total pressure of the tunnel air can be varied from a minimum value of 0.25 atmosphere at all test Mach numbers to a maximum value of 2.0 atmospheres at Mach numbers up to 0.4 and about 1.5 atmospheres at transonic Mach numbers. The tunnel air is dried sufficiently to avoid condensation effects.

Model

The models used in the present investigation were sting-supported 1/2-scale models of the Arcas meteorological sounding rocket. Details of the models are presented in figure 1, and schlieren photographs of the forebody and centerbody juncture are presented in figure 2. The models had an ogive nose, a cylindrical centerbody, and a boattail afterbody that ended with a reflex lip. Trapezoidal double-wedge fins were used to stabilize the model. Two models differing in the length of the cylindrical centerbody were investigated. The short model had a fineness ratio of 18.2 and the long model had a fineness ratio of 23.8.

The models were investigated with fins at cant angles of 0° and 2°. The cant angle of 2° for each fin was in such a direction as to produce a positive rolling moment. The models were also investigated without fins. The fin anchors (fig. 1(b)) were used to

plug the slots in the boattailed afterbody when the short model was investigated without fins, whereas the slots were plugged with balsa and faired flush with the model skin when the long model was investigated without fins.

The investigation was conducted at a constant Reynolds number of 9.8×10^6 per meter (3.0×10^6 per foot) through the Mach number range. Both models were investigated at Mach numbers of 0.60, 0.80, 0.90, 1.00, and 1.20. The short model was also investigated at a Mach number of 0.95. Tests were made through an angle-of-attack range from approximately -3° to 21° at roll angles (the strain-gage balance was not rolled during the test) of 0°, 22.5°, and 45° clockwise as viewed upstream aft of the model. In order to obtain turbulent flow over the model, a 0.25-cm-wide (0.10-in.) strip of No. 120 carborundum grains was affixed around the model 3.17 cm (1.25 in.) aft of the nose and 1.27 cm (0.5 in.) aft of the leading edge of each fin. The stagnation temperature was maintained at 322° K (120° F) at all Mach numbers during the investigation.

Measurements

Aerodynamic forces and moments were measured by means of a six-component electrical strain-gage balance housed within the model. The balance was rigidly fastened to a 2.54-cm-diameter (1-in.) sting support which extended 29.21 cm (11.5 in.) aft of the model base and ended with a 19.2° half-angle flare attached to the tunnel sting.

Corrections

Angles of attack were corrected for tunnel-flow angularity and balance and sting-support-system deflection under aerodynamic load. Axial-force data were not corrected to free-stream conditions at the model base, except for the summary data at a roll angle of 0° and an angle of attack of 0°.

Accuracy

The accuracy of the individual measured quantities, based on calibrations and repeatability of data, is estimated to be within the following limits:

C_A	±0.004	C_Y	±0.03
C_l	±0.01	$C_{p,b}$	±0.01
C_m	±0.05	α, deg	±0.1
C_n	±0.05	ϕ, deg	±0.5
C_N	±0.03	M	±0.003

PRESENTATION OF RESULTS

A list of the basic figures presenting the results of the investigation is presented in the following table:

Model	Fin cant angle, deg	$C_{p,b}$	C_A	C_N	C_m	C_Y	C_n	C_l
		Figure						
Short	0	3	7(a)	7(b)	7(c)	7(d)	7(e)	7(f)
Short	2	4	8(a)	8(b)	8(c)	8(d)	8(e)	8(f)
Long	0	5	9(a)	9(b)	9(c)	9(d)	9(e)	9(f)
Long	2	6	10(a)	10(b)	10(c)	10(d)	10(e)	10(f)

Summary data figures of the variation with Mach number of the center-of-pressure location in percent body length, the axial-force coefficient corrected to free-stream conditions at the model base, and the base axial-force coefficient are presented in figure 11 for the short model and in figure 12 for the long model.

DISCUSSION

Axial Force

The variation of the axial-force coefficient with angle of attack is presented in figures 7(a) and 8(a) for the short model and in figures 9(a) and 10(a) for the long model. These coefficients are not corrected for the base axial force; however, base pressure coefficients for both models are presented in figures 3 to 6. The variation with Mach number of the base axial-force coefficient $C_{A,b}$ and of the axial-force coefficient corrected for base axial force $C_{A,corr}$ for the short model without fins and with fins at cant angles of 0° and 2° is shown in figure 11 for $\alpha \approx 0^\circ$. The base axial-force coefficients were generally negative at Mach numbers less than 1.00 and were positive at a Mach number of 1.20. This trend is characteristic of boattailed afterbodies and is also associated with sting diameter and flare angle. (See ref. 2.) The variation of $C_{A,b}$ and $C_{A,corr}$ with Mach number is shown in figure 12 for the long model at $\alpha \approx 0^\circ$. The trend is generally the same as that for the short model; however, the base axial-force coefficient is negative for the fins-off configuration at a Mach number of 1.20. The positive base axial-force coefficient at $M = 1.20$ for the short model is probably attributable to the fin anchors. A comparison of the fins-off configurations for the long and short models indicates that the long model has higher $C_{A,corr}$ coefficients than the short model at Mach numbers from 0.60 to 0.975. At Mach numbers from 0.975 to 1.20,

the short model has higher $C_{A,corr}$ values. This trend is also attributed to the fin anchors, which were not flush with the model skin on the short model.

Normal Force

The results shown in figures 7(b), 8(b), 9(b), and 10(b) indicate that the slope of the normal-force-coefficient curve increases with angle of attack for the model without fins. This trend is characteristic of slender bodies and is associated with viscous lift (ref. 3). This effect is therefore greater for the longer body since a common reference area was used.

Pitching Moment

The short model and long model had similar pitch-up tendencies in the angle-of-attack range from 8° to 16° at all roll positions of the fins. (See figs. 7(c), 8(c), 9(c), and 10(c).) The roll positions of 22.5° and 45° of the fins generally delayed the pitch-up to higher angles of attack at Mach numbers 0.60, 0.80, 0.90, and 0.95. At a Mach number of 1.00, the pitch-up occurred at lower angles of attack for the 45° roll position than for either of the other roll positions of the fins. At a Mach number of 1.20, the roll position of the fins had little effect on the pitch-up tendencies of the model. Figure 7(c) indicates that the longitudinal static stability of the short model with fin cant angle of 0° is almost neutral in the angle-of-attack range from -2° to 2° at Mach numbers of 0.60, 0.80, and 0.90. This characteristic is considerably improved with the fins canted to 2° (fig. 8(c)).

Center of Pressure

The variation of center-of-pressure location with Mach number for the short model at a roll angle of 0° and small angles of attack, within the range of linear aerodynamics, is shown in figure 11. The fin cant angle of 2° moved the center of pressure rearward at Mach numbers from 0.60 to approximately 1.00 and forward at Mach numbers from approximately 1.00 to 1.20. The fin cant angle had little effect on the center-of-pressure location for the long model (fig. 12).

Side Force and Yawing Moment

The side-force coefficients were generally small up to an angle of attack of 16°; at angles of attack greater than 16°, the side-force coefficients were either positive or negative, depending on the roll position of the fins, the Mach number, and the model length. (See figs. 7(d), 8(d), 9(d), and 10(d).)

The yawing-moment coefficients were generally small at angles of attack less than 12°. At angles of attack greater than 14°, the yawing-moment data are erratic for

some of the roll positions of the fins and large values were obtained for the long model with the fins canted 2° (fig. 10(e)).

The data presented in references 4 and 5 at subsonic speeds indicate that asymmetric trailing vortices produced by the forebody of high-fineness-ratio bodies of revolution, at large angles of attack, result in large side forces and large yawing moments on the body. The experimental data presented in reference 6 at a Mach number of 1.91 indicate that large sidewash angles caused by the trailing vortices are present at angles of attack above 10°. Therefore, it is believed that the large side forces and large yawing moments on the long model at angles of attack greater than 12° are caused by asymmetric vortices on the leeward side of the model, generated by the ogive nose and forebody. At small angles of attack, these vortices are formed at the same body station on both sides of the body and are symmetrical. As a result, the side forces and yawing moments obtained at these conditions are small. At angles of attack greater than 14°, the vortices on opposite sides of the body are formed at different body stations, are asymmetric, and cause large yawing moments and side forces on the body at 0° sideslip angle. The coefficients frequently change sign with small changes in angle of attack at angles of attack greater than 14°. These trends are present for the models without fins as well as for the models with fins (figs. 10(d) and 10(e)) and are a result of the asymmetric vortices. Schlieren photographs of the vortices are shown in figure 2 at angles of attack of approximately 17.3° and 22.4°. With the schlieren knife edge horizontal, changes in density gradient through the vortices result in a dark band on one side of the vortex and a light band on the other.

Rolling Moment

The canted fins were effective in producing a positive rolling-moment coefficient on the short model (fig. 8(f)) in the angle-of-attack range from -4° to 12°. At angles of attack greater than 8°, the rolling-moment coefficient generally decreased for the roll positions of 0° and 45° and in several instances slightly negative values were measured. The rolling-moment coefficient increased with angle of attack for the roll angle of 22.5° in the angle-of-attack range from approximately 13° to 17°. The trend in the variation of rolling-moment coefficient with angle of attack for the long model was similar to that of the short model.

CONCLUSIONS

Static stability tests at Mach numbers from 0.60 to 1.20 of a 1/2-scale model of a meteorological sounding rocket with variations in body length, fin cant angle, and roll angle led to the following conclusions:

1. At all Mach numbers and roll positions of this investigation, the models had similar pitch-up tendencies in the angle-of-attack range from 8° to 16°.

2. The fin cant angle of 2° improved the longitudinal stability of the short model in the angle-of-attack range from -2° to 2°.

3. The asymmetric vortices from the forebody caused large yawing moments at angles of attack greater than 14°.

4. The canted fins produced positive rolling moments through the angle-of-attack range from -4° to 12° for the test roll angles at all test Mach numbers.

Langley Research Center,
National Aeronautics and Space Administration,
Langley Station, Hampton, Va., December 16, 1966,
607-06-00-01-23.

REFERENCES

1. Babb, C. Donald; and Fuller, Dennis E.: Static Stability Investigation of a Sounding-Rocket Vehicle at Mach Numbers From 1.50 to 4.63. NASA TN D-4014, 1967.

2. Cahn, Maurice S.: An Experimental Investigation of Sting-Support Effects on Drag and a Comparison With Jet Effects at Transonic Speeds. NACA Rept. 1353, 1958. (Supersedes NACA RM L56F18a.)

3. Polhamus, Edward C.: Effect of Nose Shape on Subsonic Aerodynamic Characteristics of a Body of Revolution Having a Fineness Ratio of 10.94. NACA RM L57F25, 1957.

4. Letko, William: A Low-Speed Experimental Study of the Directional Characteristics of a Sharp-Nosed Fuselage Through a Large Angle-of-Attack Range at Zero Angle of Sideslip. NACA TN 2911, 1953.

5. Dunn, Eldon L.: A Low-Speed Experimental Study of Yaw Forces on Bodies of Revolution at Large Angles of Pitch and Zero Angle of Sideslip. TM-1588, U.S. Naval Ord. Test Station, Mar. 1954.

6. Raney, D. J.: Measurement of the Cross Flow Around an Inclined Body at a Mach Number of 1.91. Tech. Note No. Aero 2357, Brit. R.A.E., Jan. 1955.

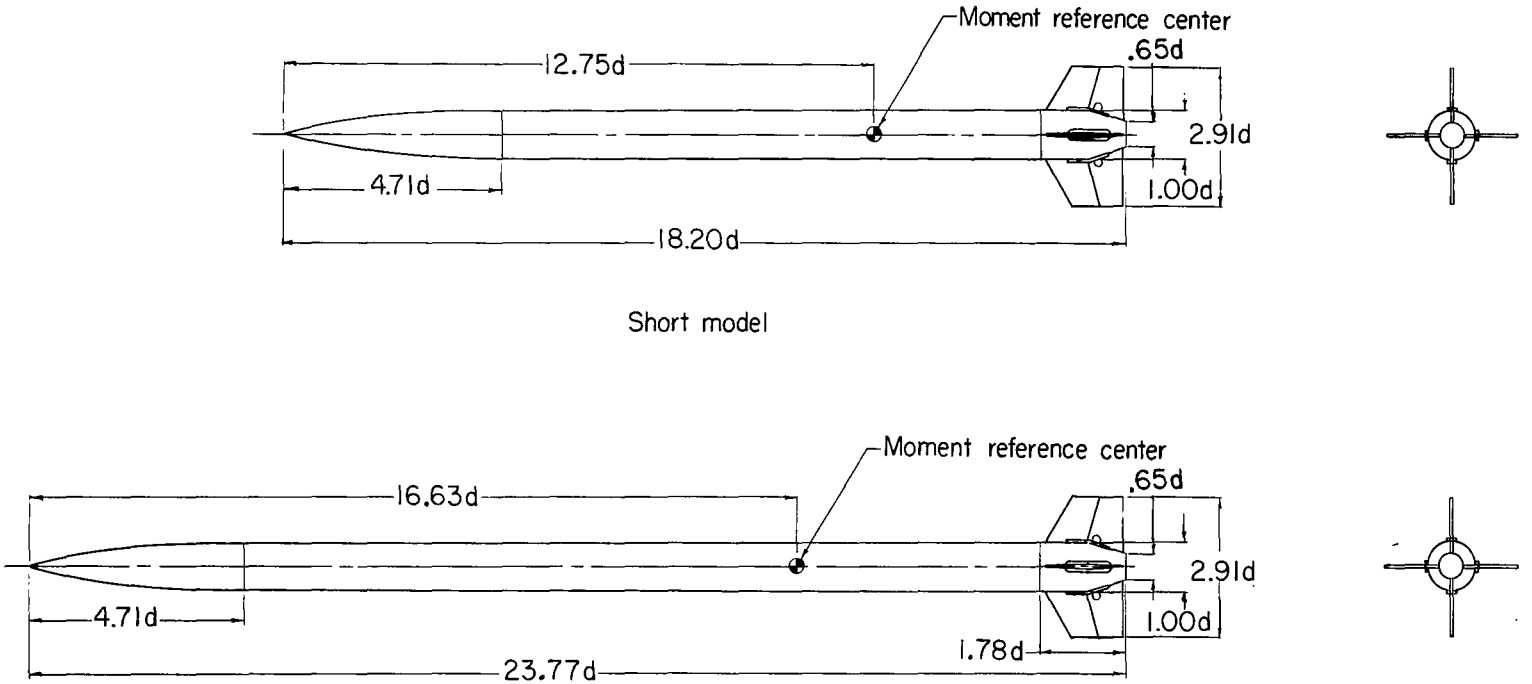

(a) General arrangement of short and long models.

Figure 1.- Model geometric characteristics. All dimensions are in terms of centerbody diameter d, 5.72 cm (2.25 in.).

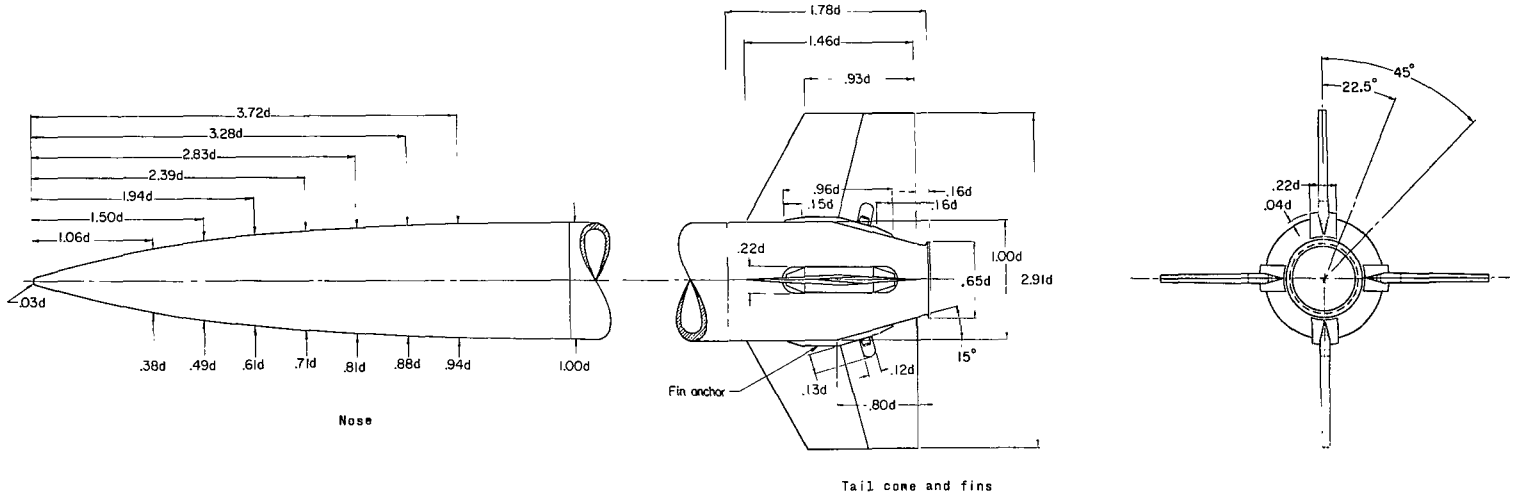

(b) Details of forebody, tail cone, and fins.

Figure 1.- Concluded.

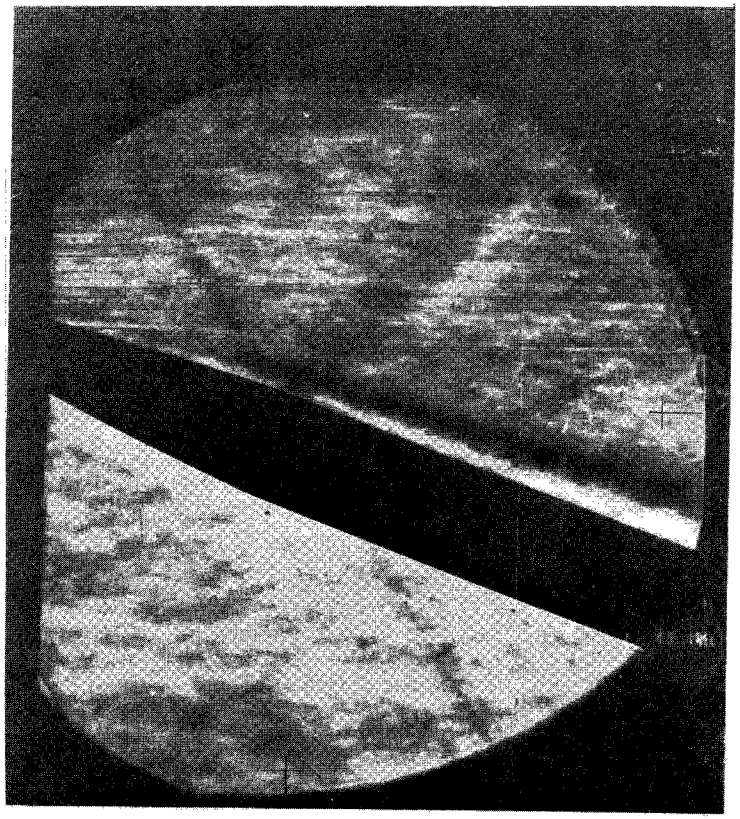

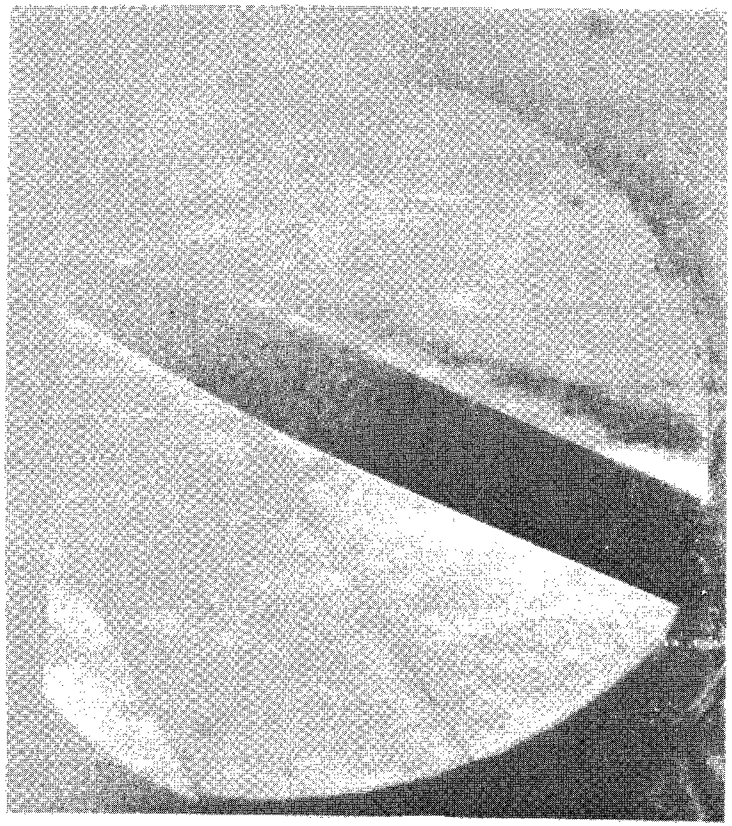

Figure 2.- Schlieren photographs of forebody and centerbody juncture. M = 1.20; $\Phi = 0^0$; long model. Knife edge horizontal. L-67-922

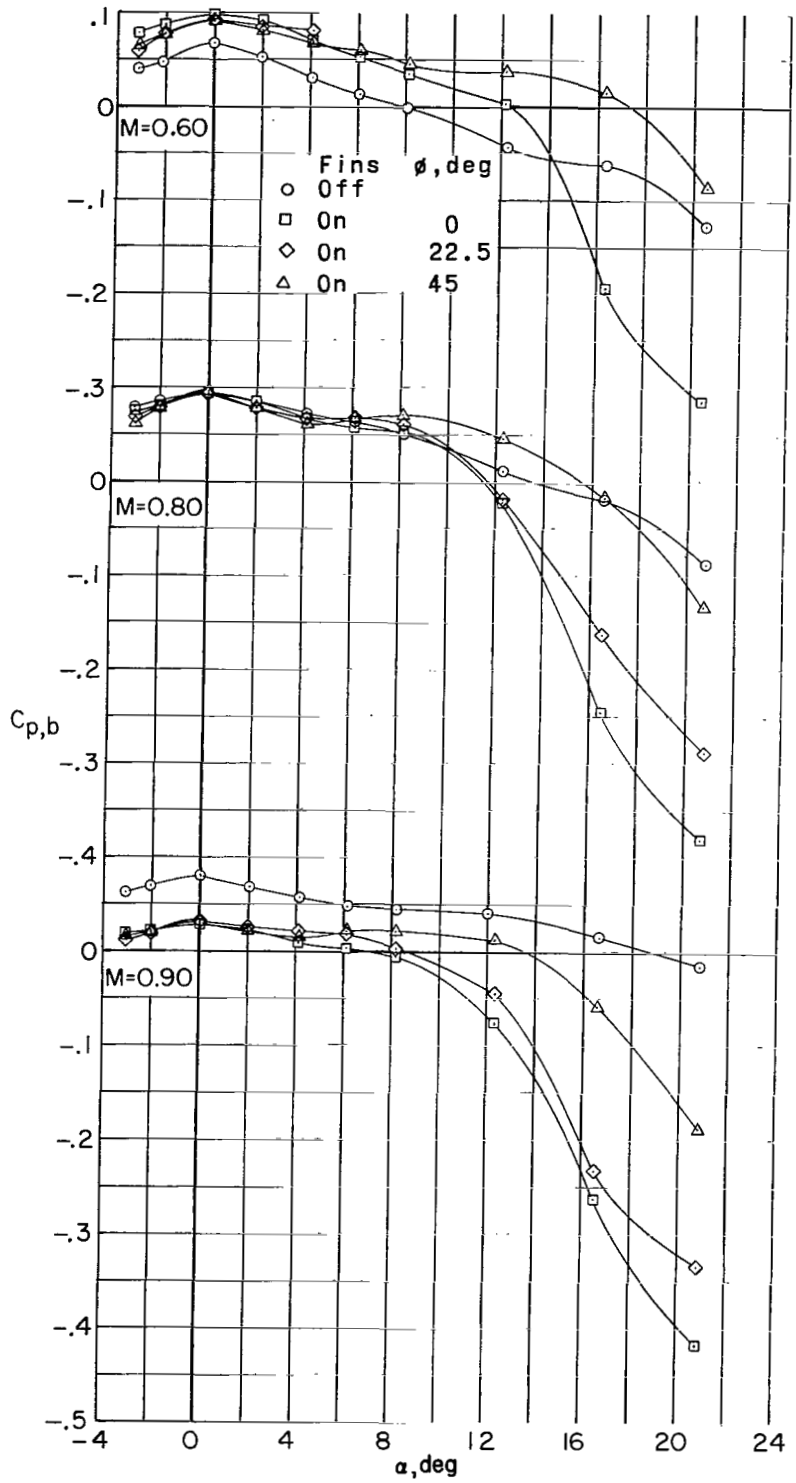

Figure 3.- Effect of roll angle on base pressure coefficient. Short model; $\delta_F = 0^0$.

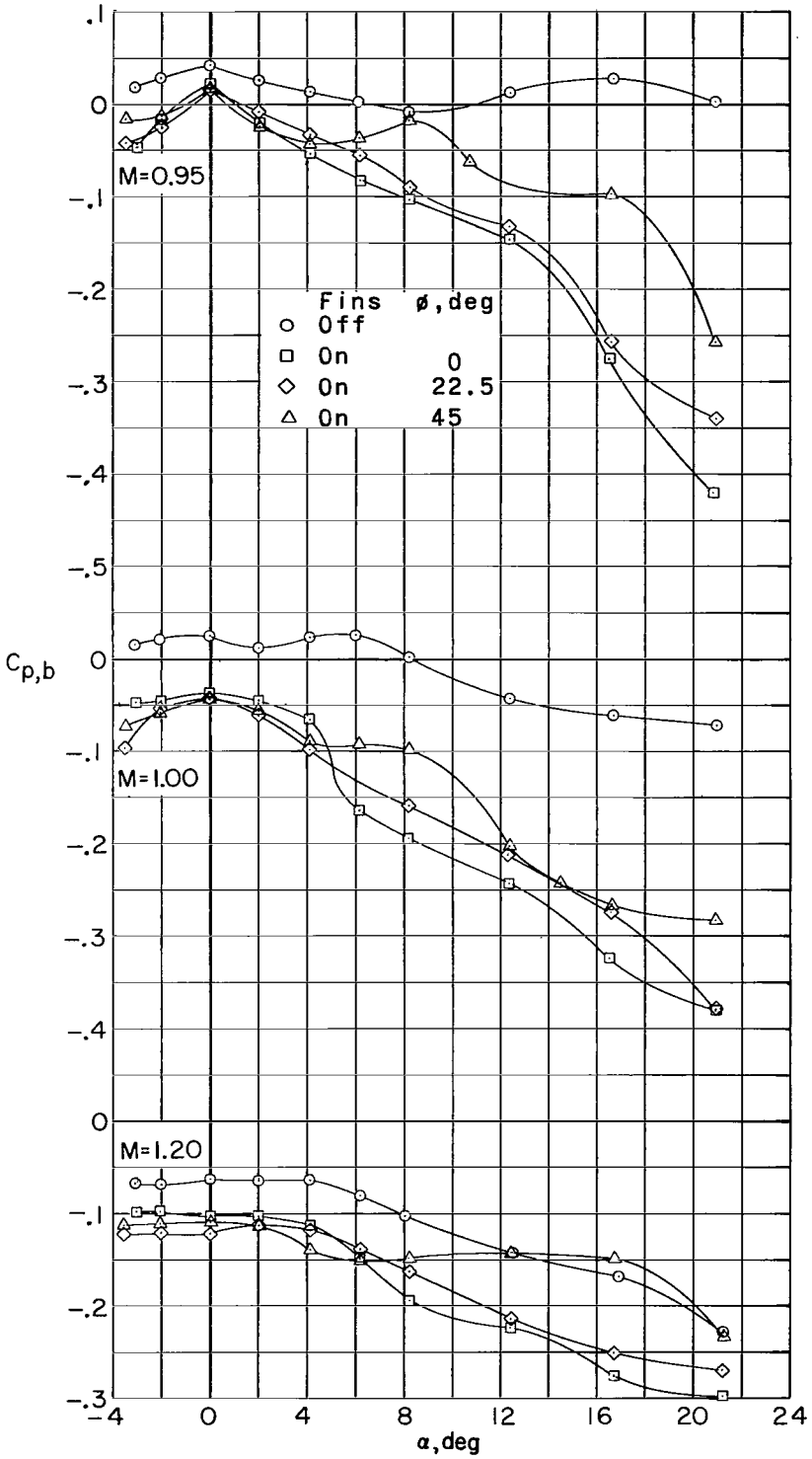

Figure 3.- Concluded.

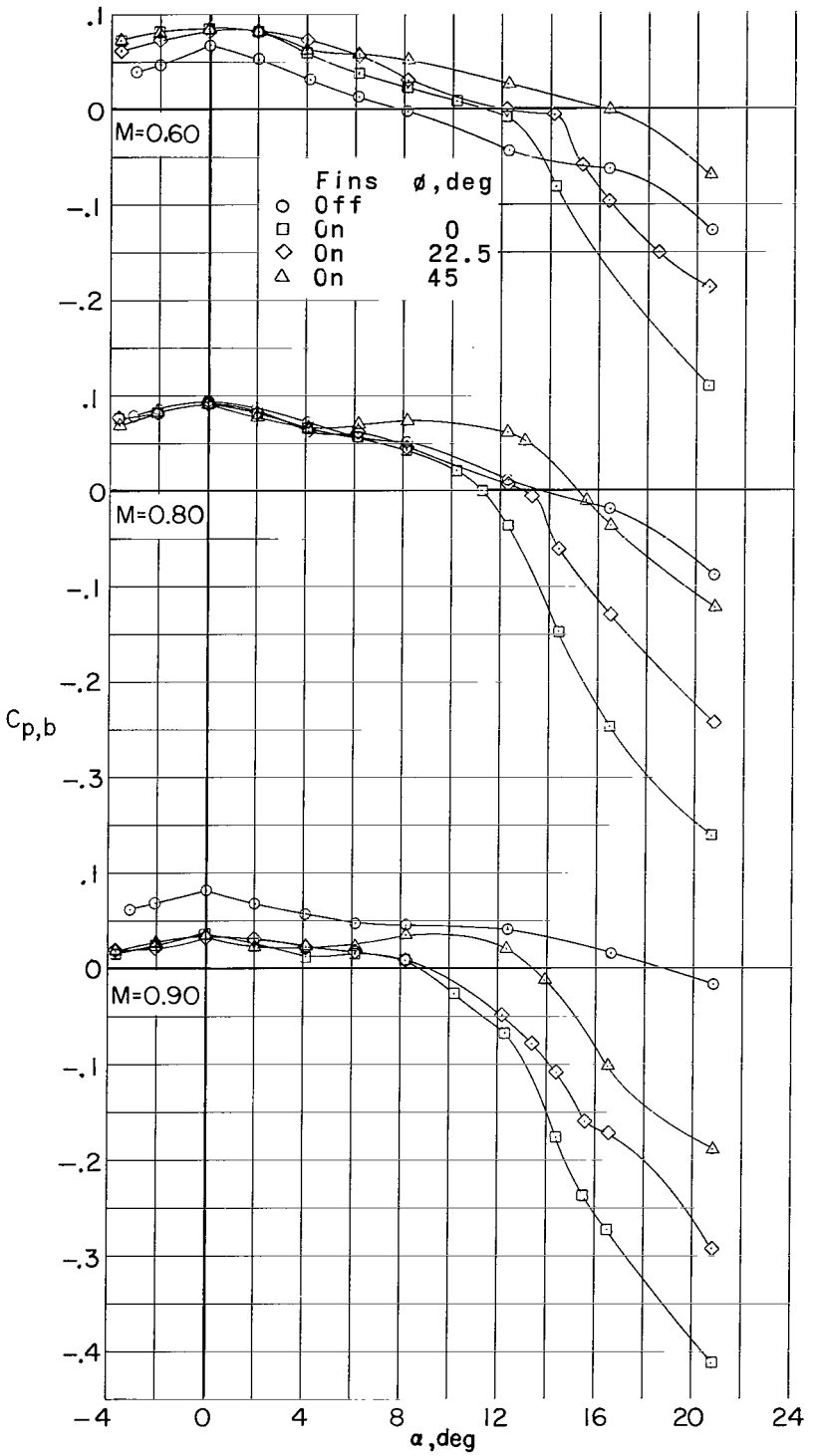

Figure 4.- Effect of roll angle on base pressure coefficient. Short model; $\delta_F = 2^0$.

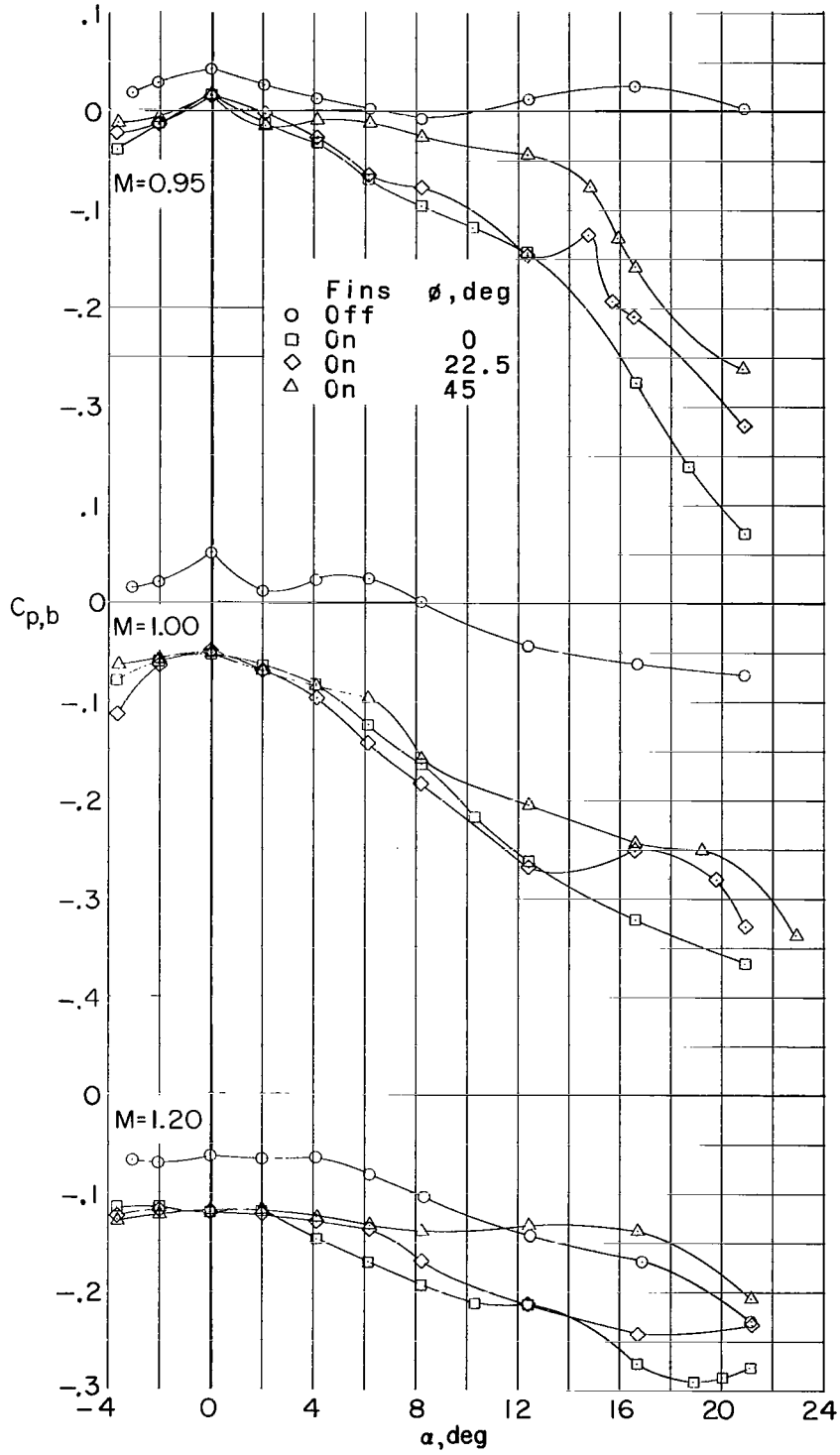

Figure 4.- Concluded.

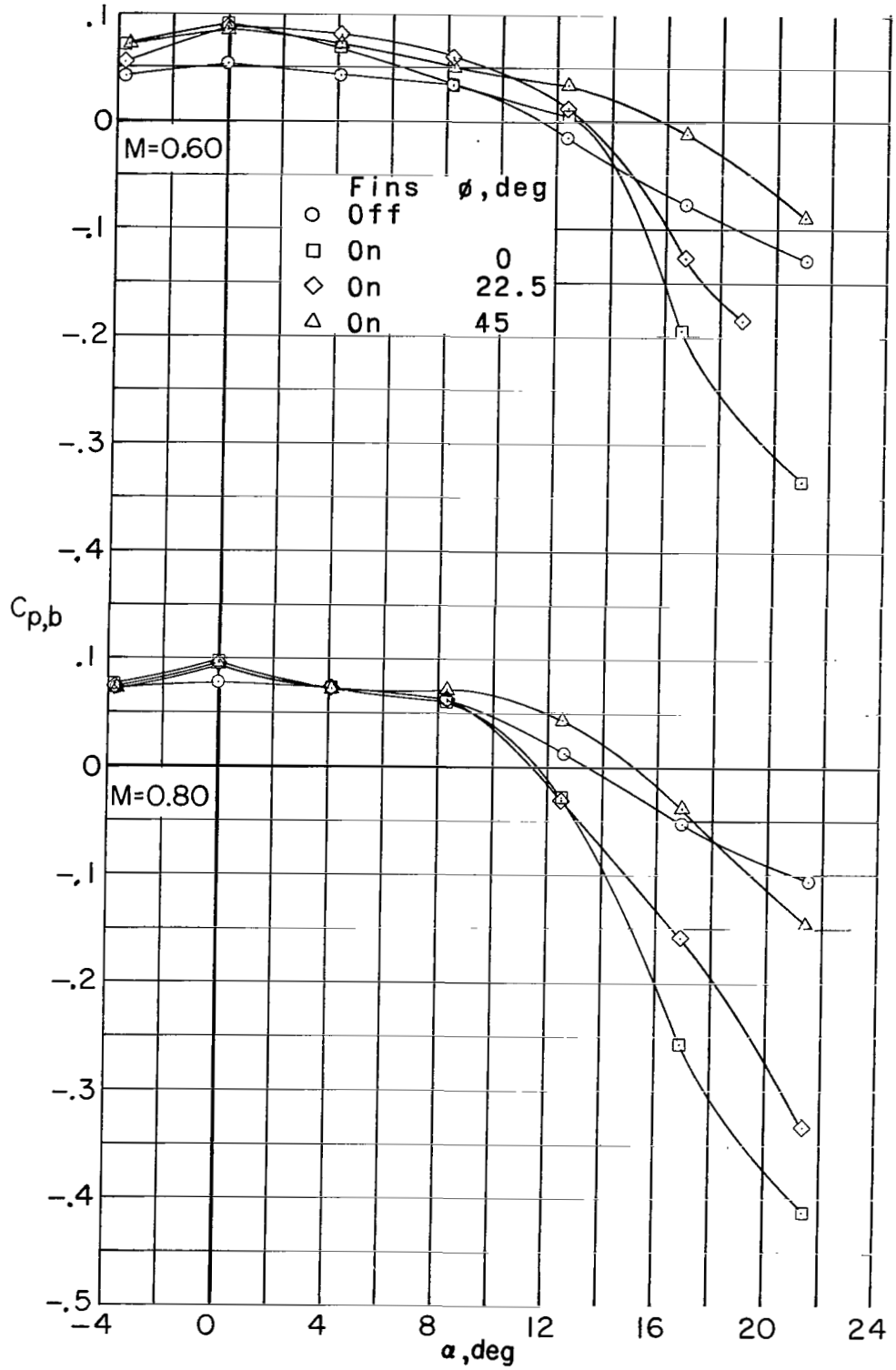

Figure 5.- Effect of roll angle on base pressure coefficient. Long model; $\delta_F = 0^0$.

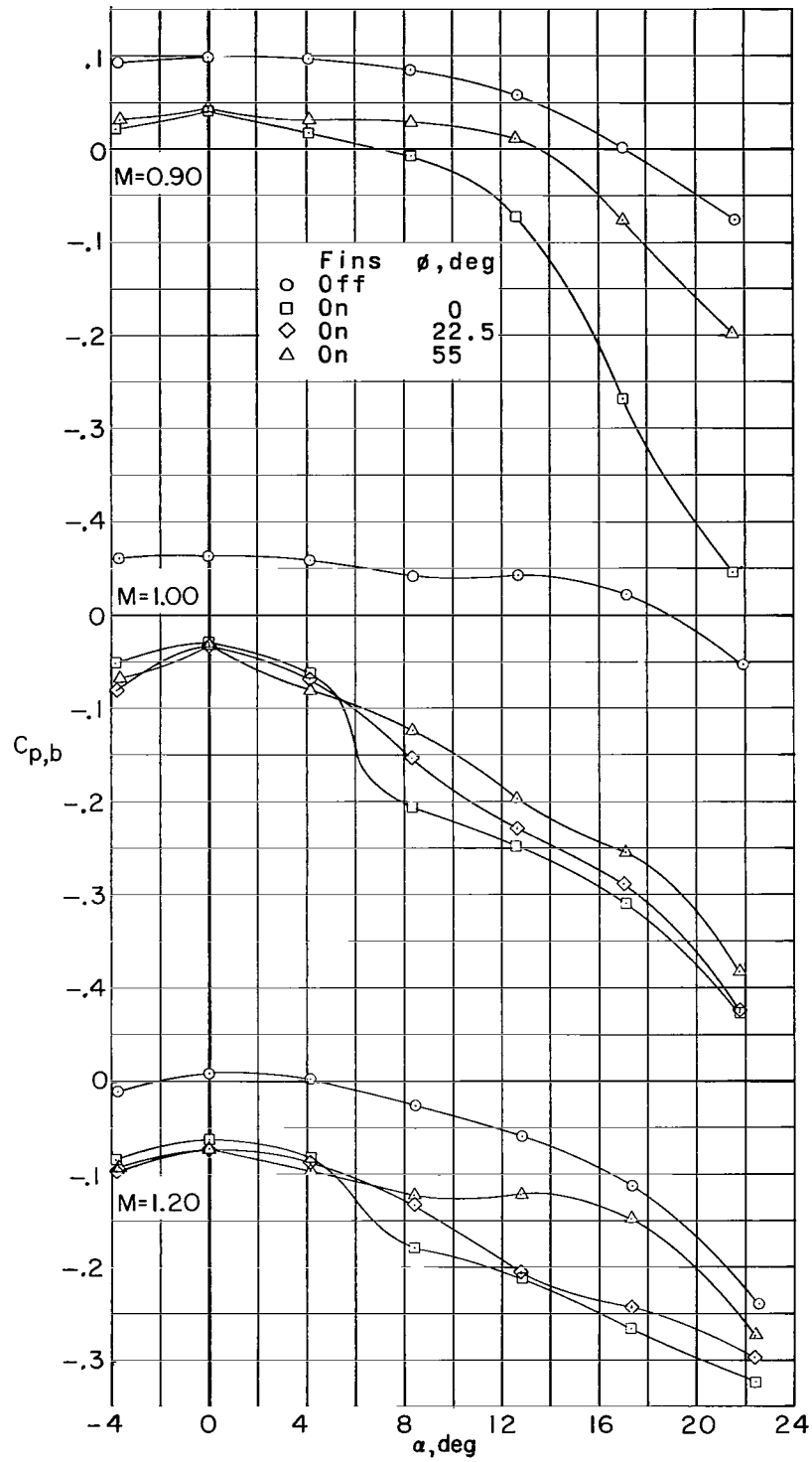

Figure 5.- Concluded.

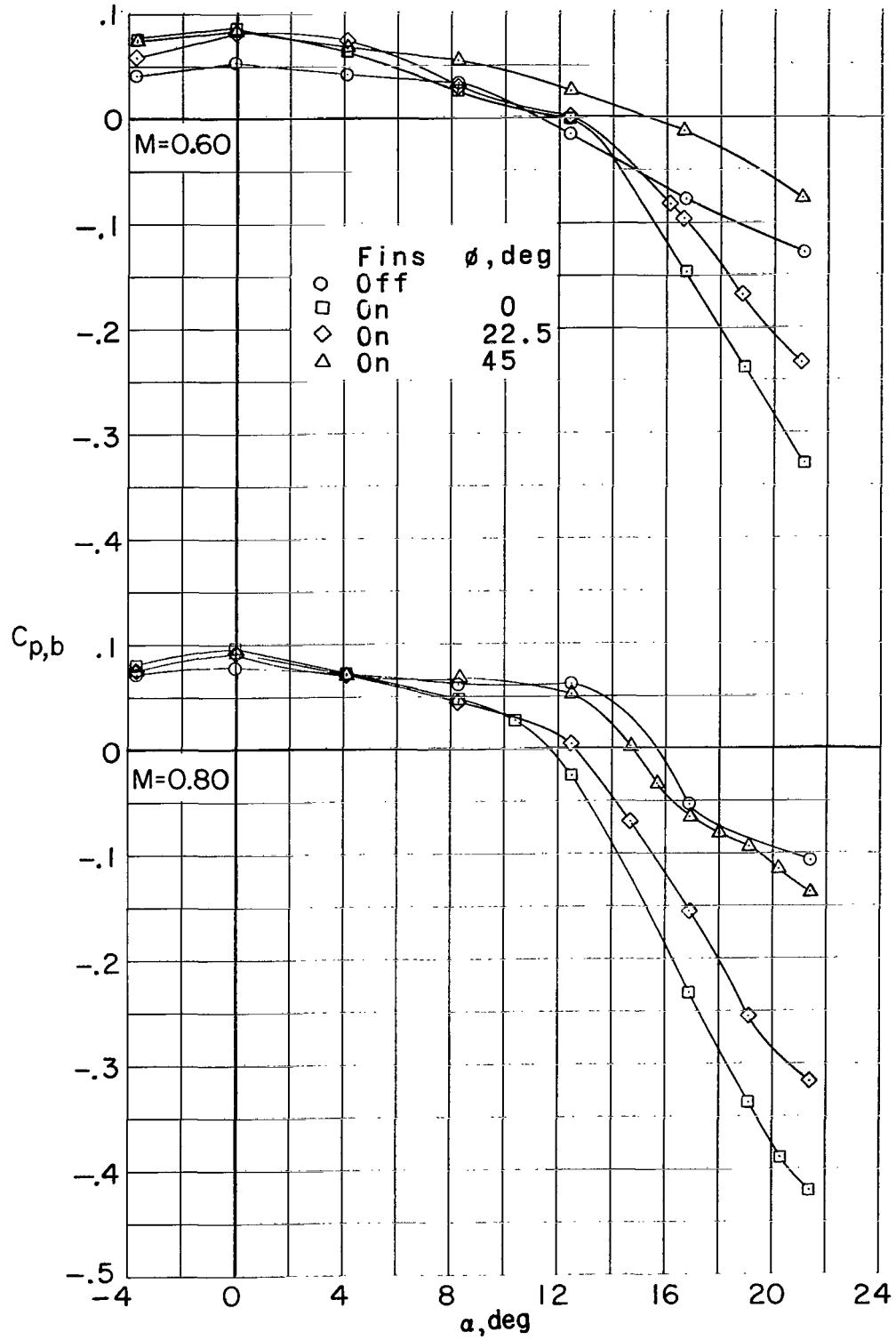

Figure 6.- Effect of roll angle on base pressure coefficient. Long model; $\delta_F = 2^0$.

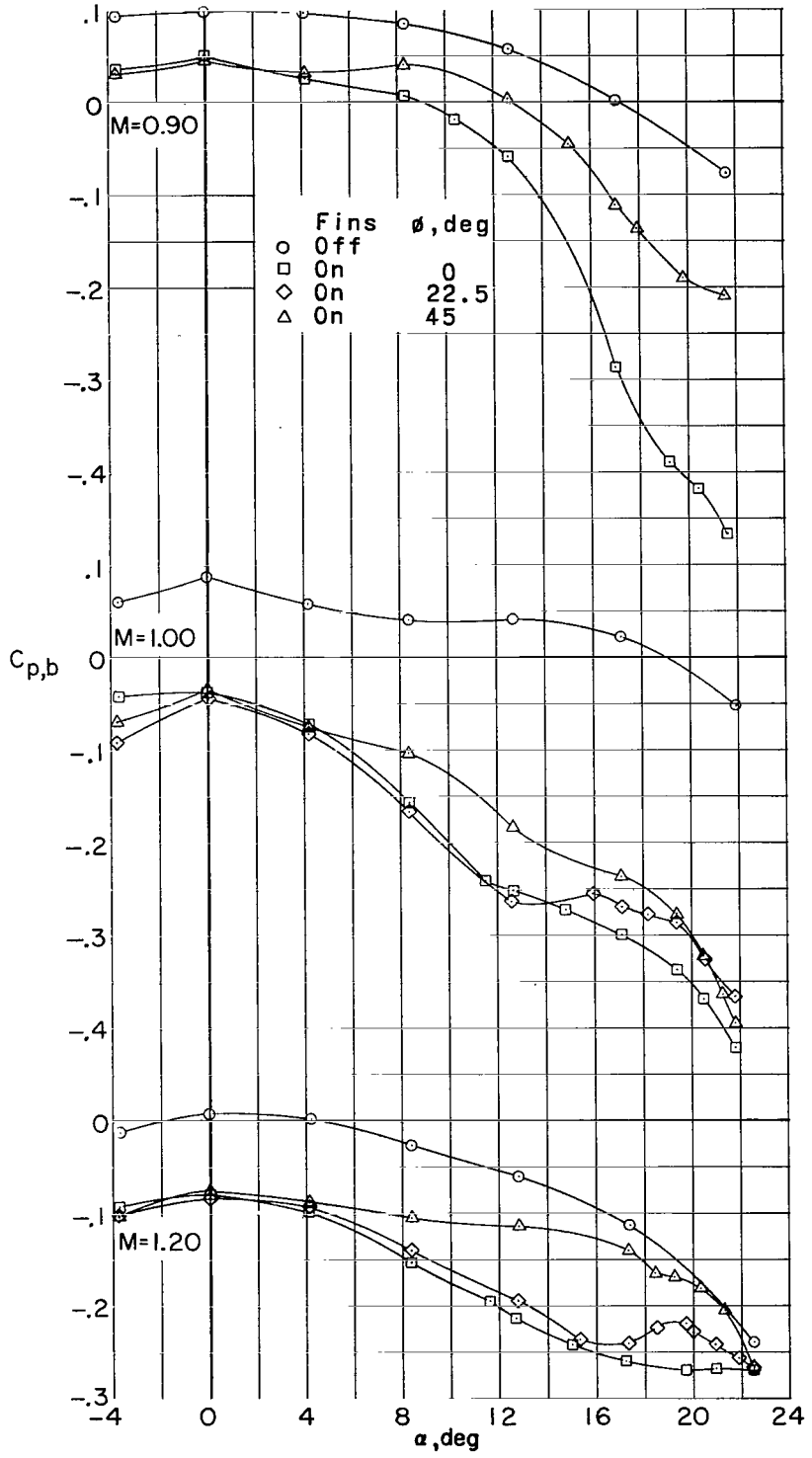

Figure 6.- Concluded.

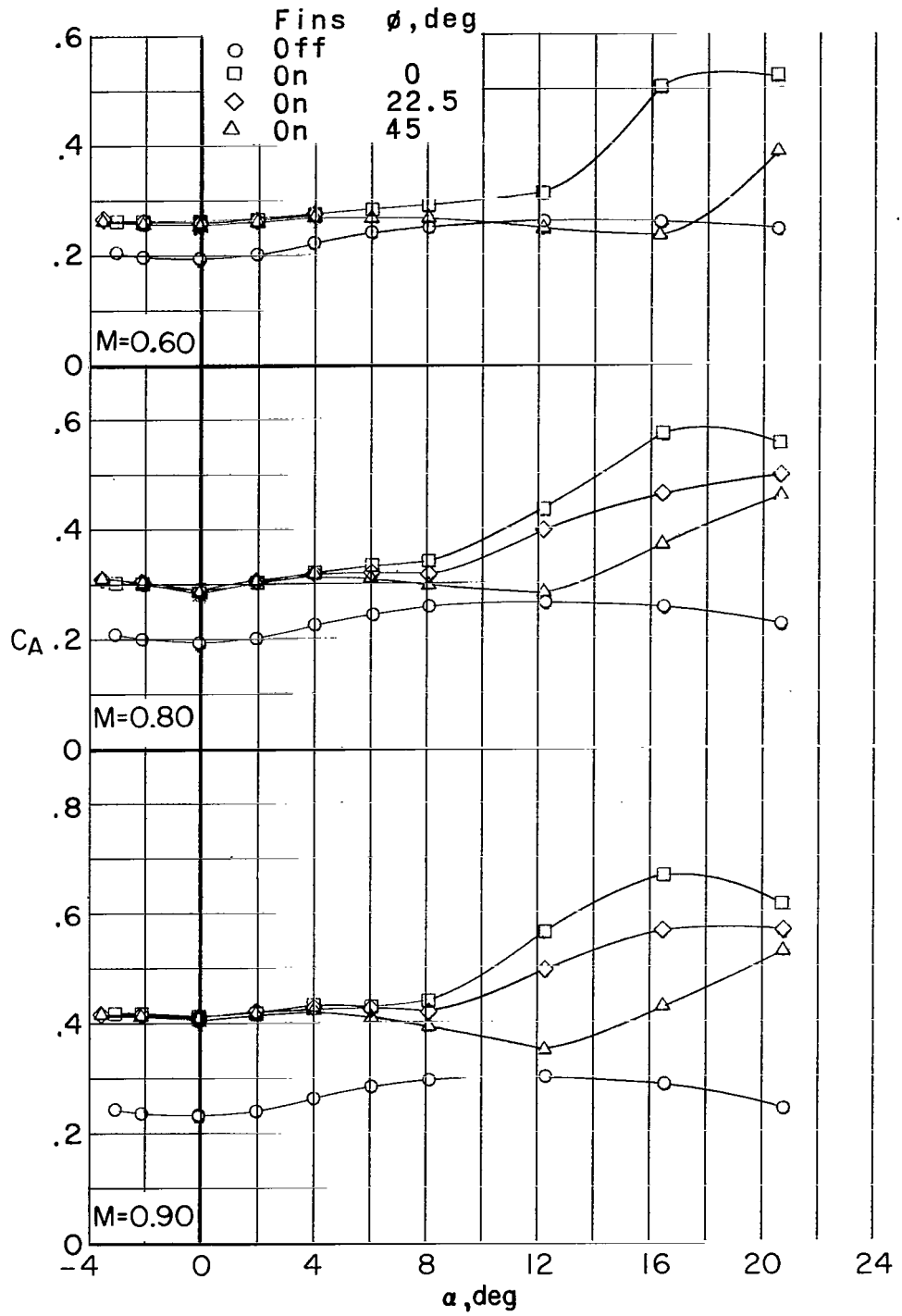

(a) Axial-force coefficient.

Figure 7.- Effect of roll angle on aerodynamic characteristics. Short model; $\delta_F = 0^o$.

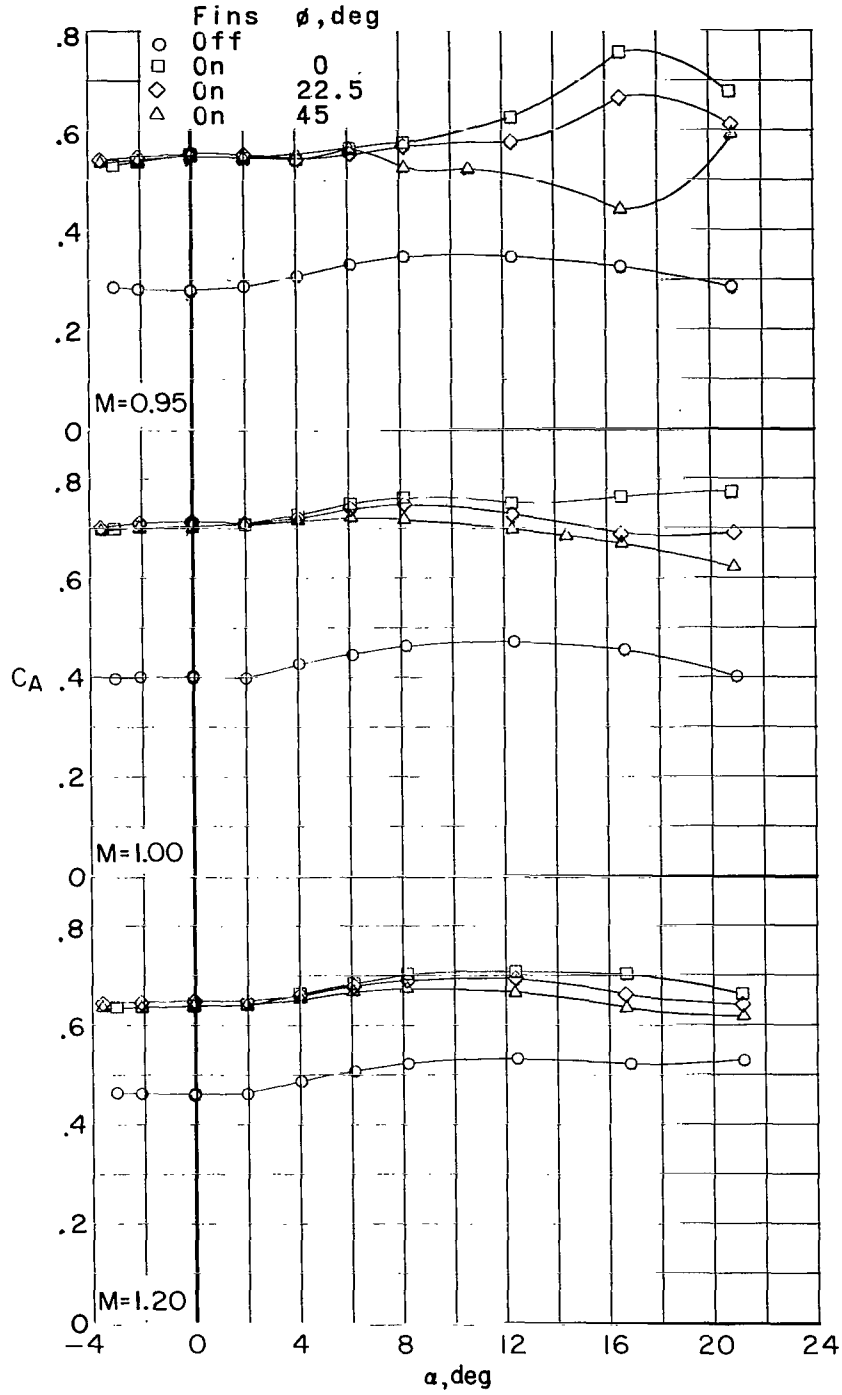

(a) Concluded.

Figure 7.- Continued.

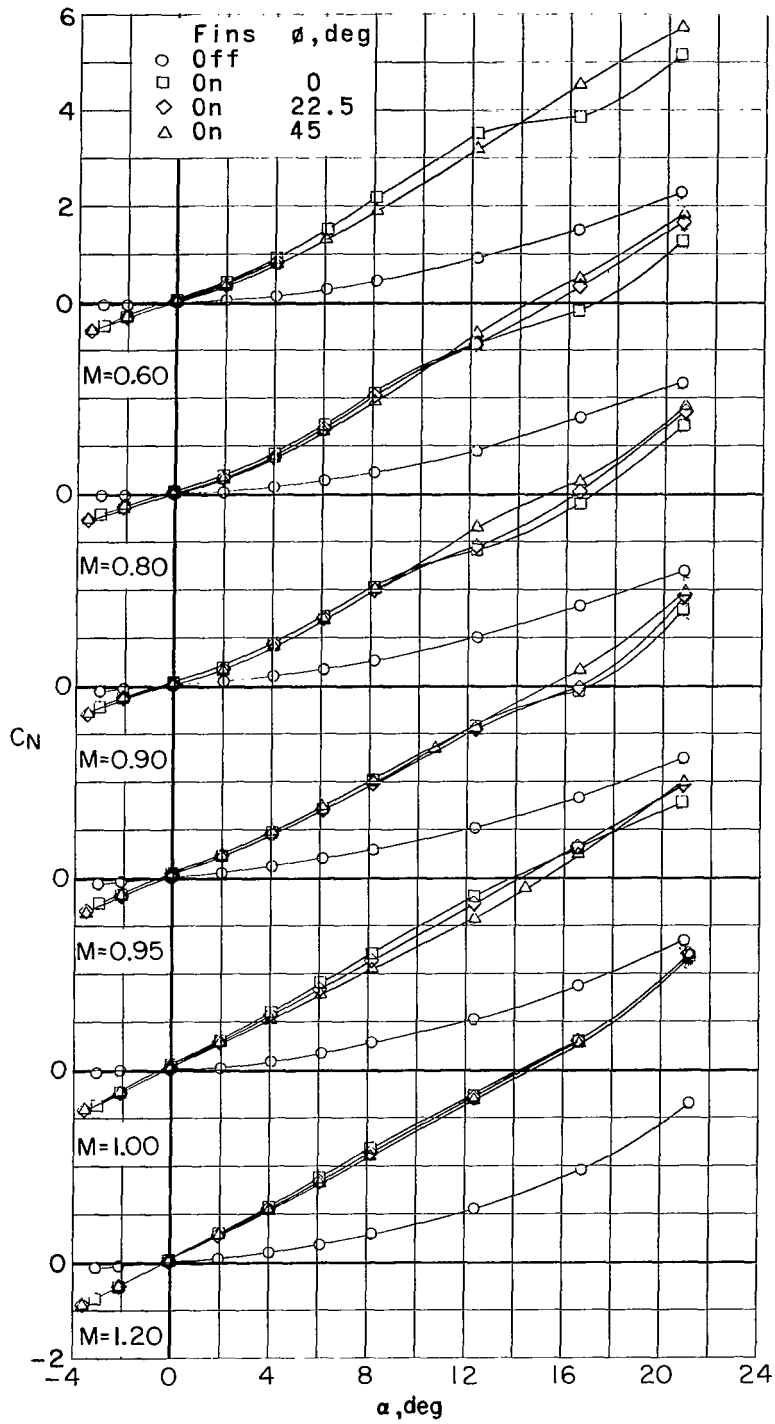

(b) Normal-force coefficient.

Figure 7.- Continued.

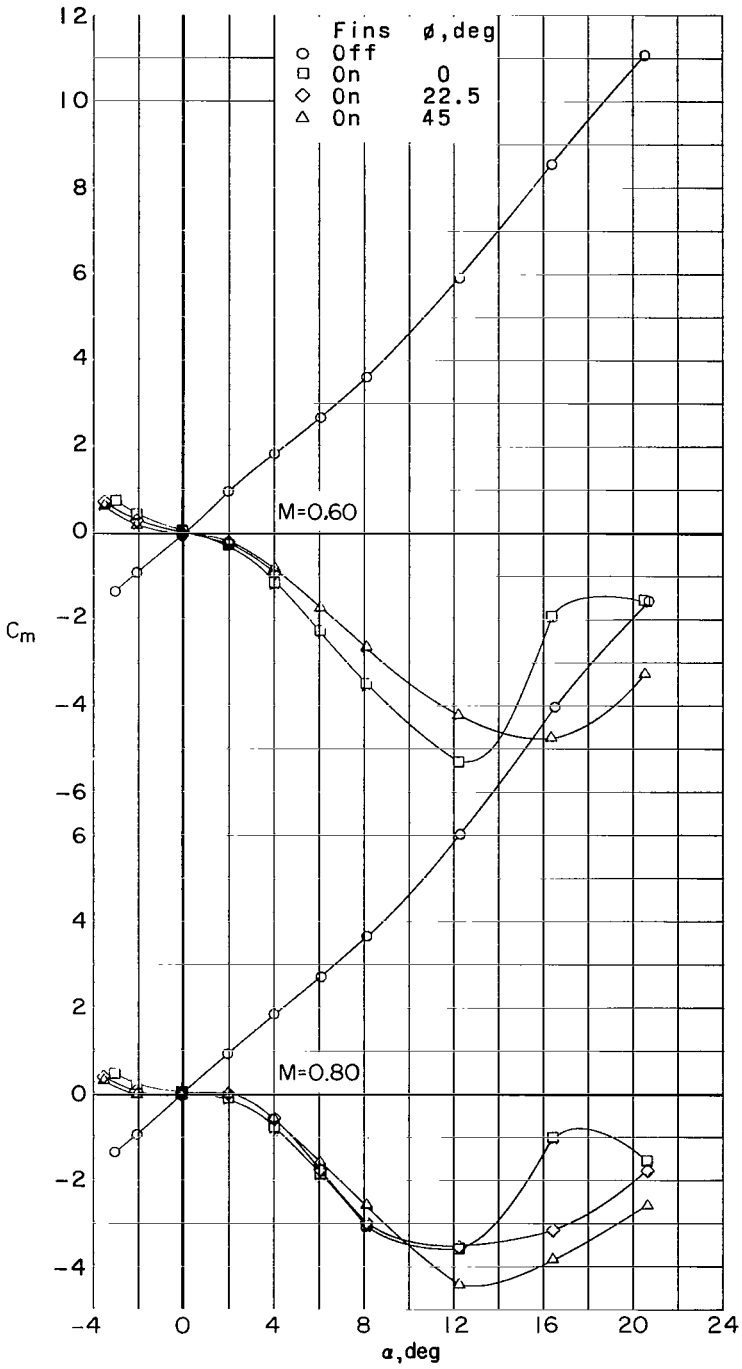

(c) Pitching-moment coefficient.

Figure 7.- Continued.

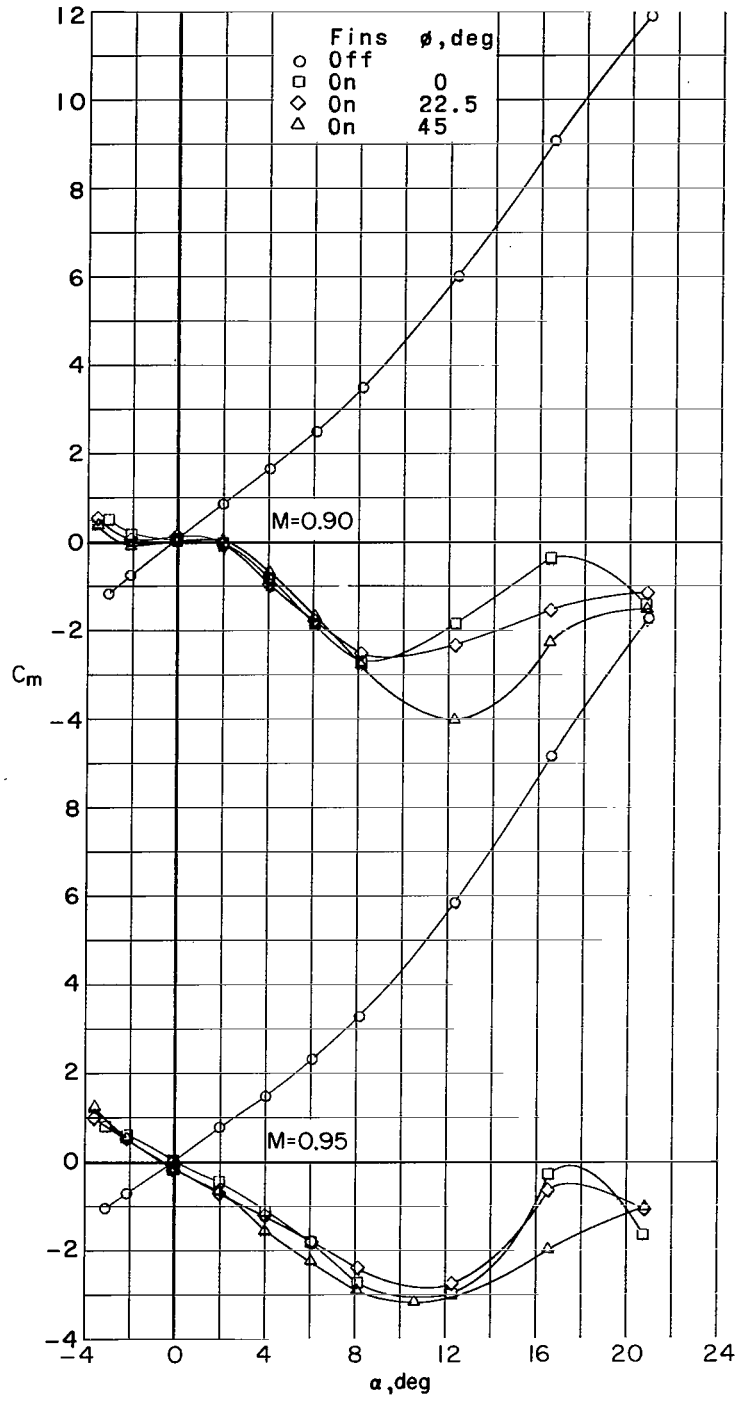

(c) Continued.

Figure 7.- Continued.

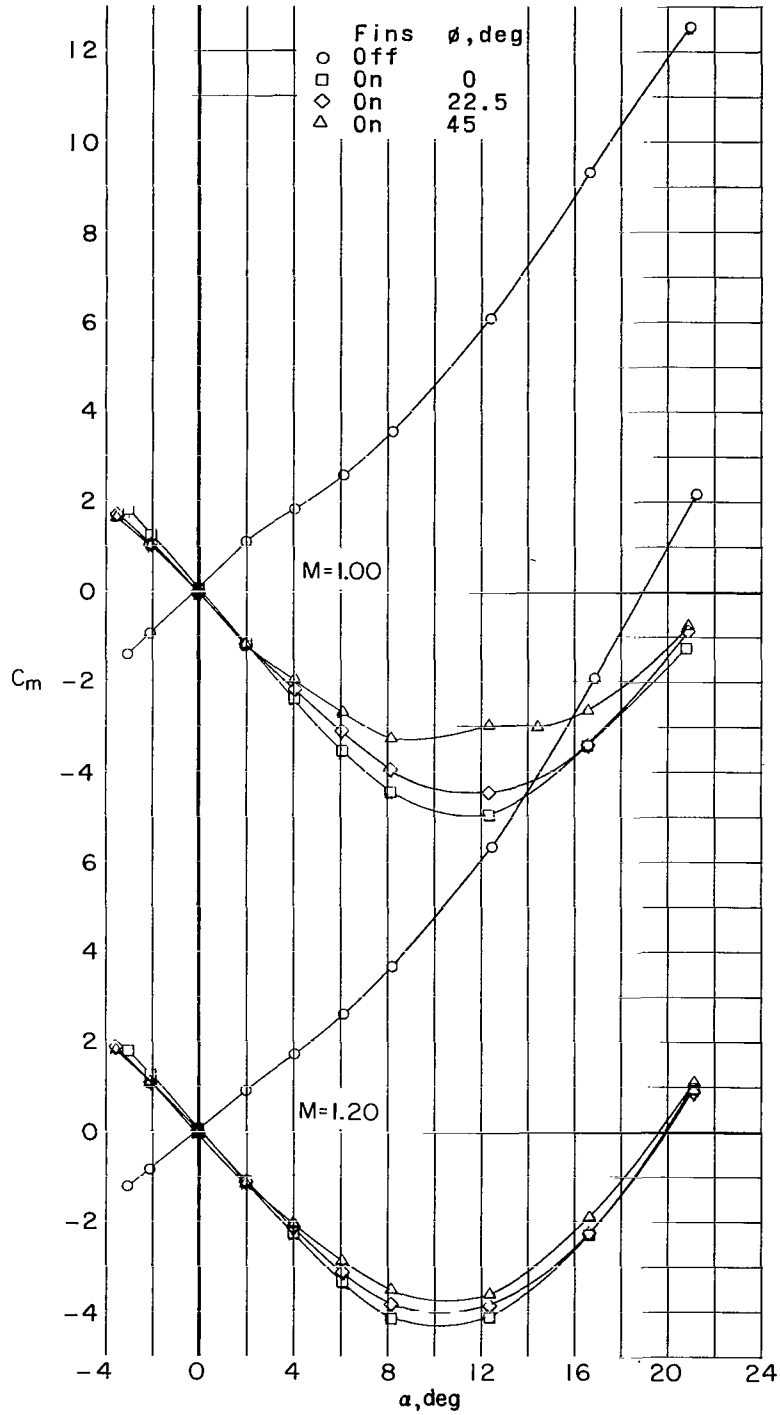

(c) Concluded.

Figure 7.- Continued.

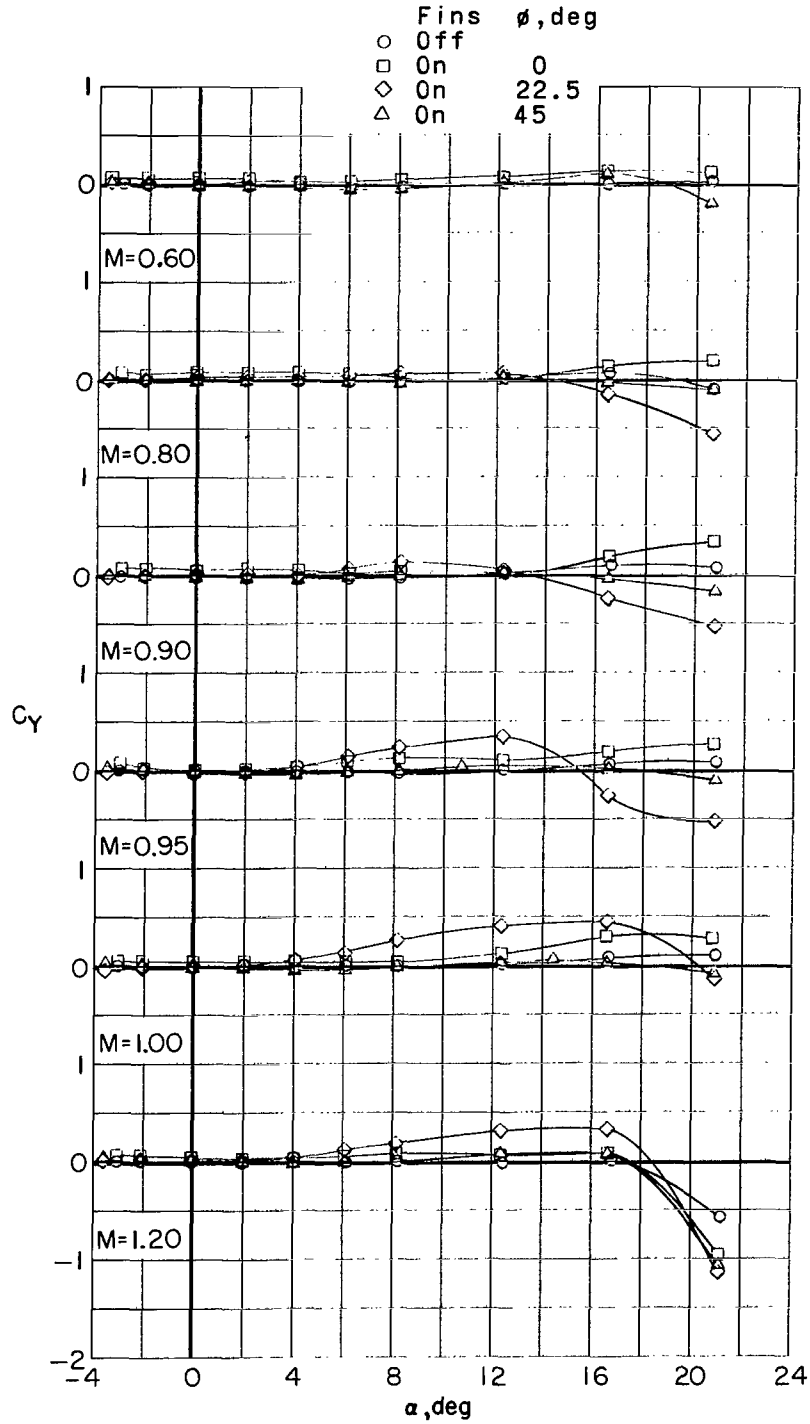

(d) Side-force coefficient.

Figure 7.- Continued.

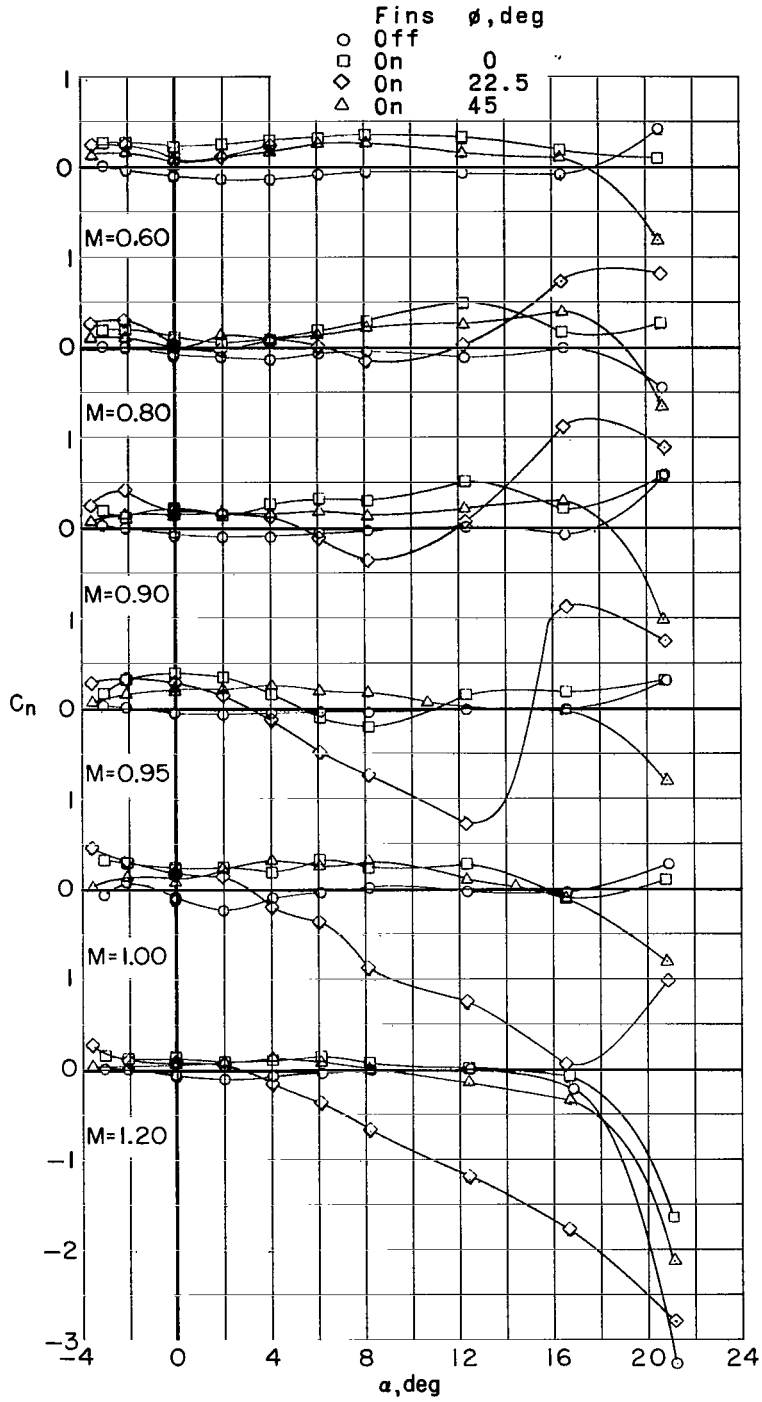

(e) Yawing-moment coefficient.

Figure 7.- Continued.

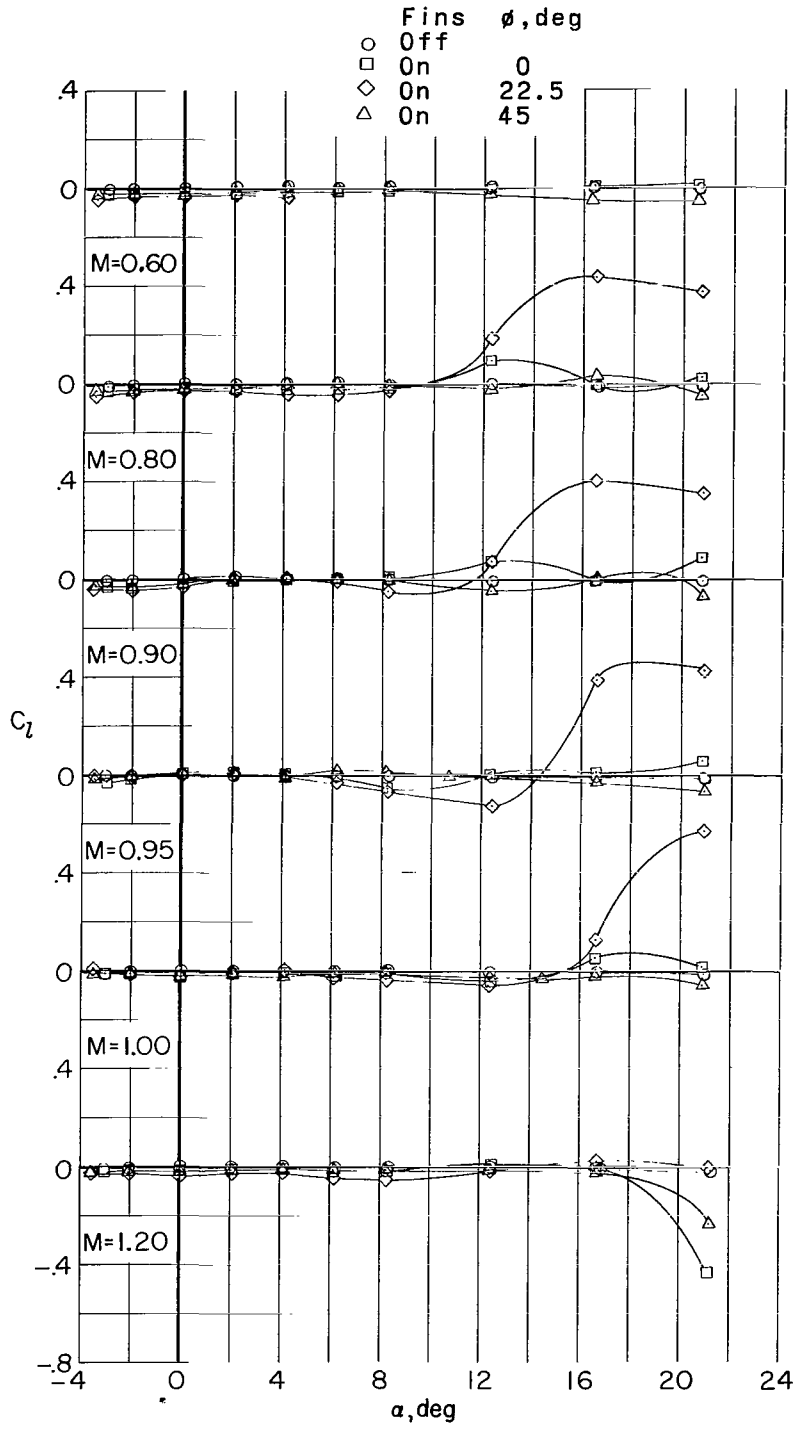

(f) Rolling-moment coefficient.

Figure 7.- Concluded.

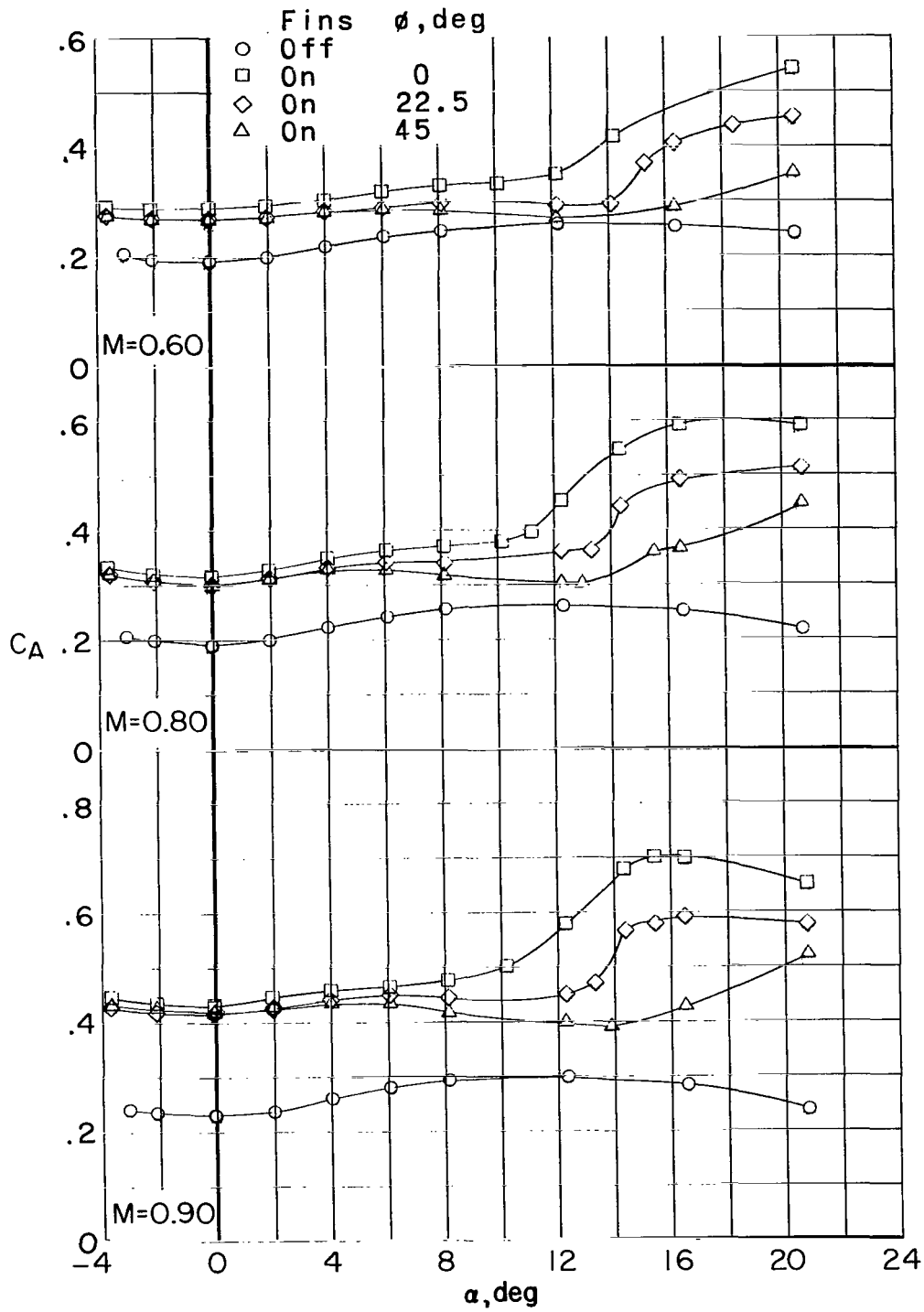

(a) Axial-force coefficient.

Figure 8.- Effect of roll angle on aerodynamic characteristics. Short model; $\delta_F = 2^0$.

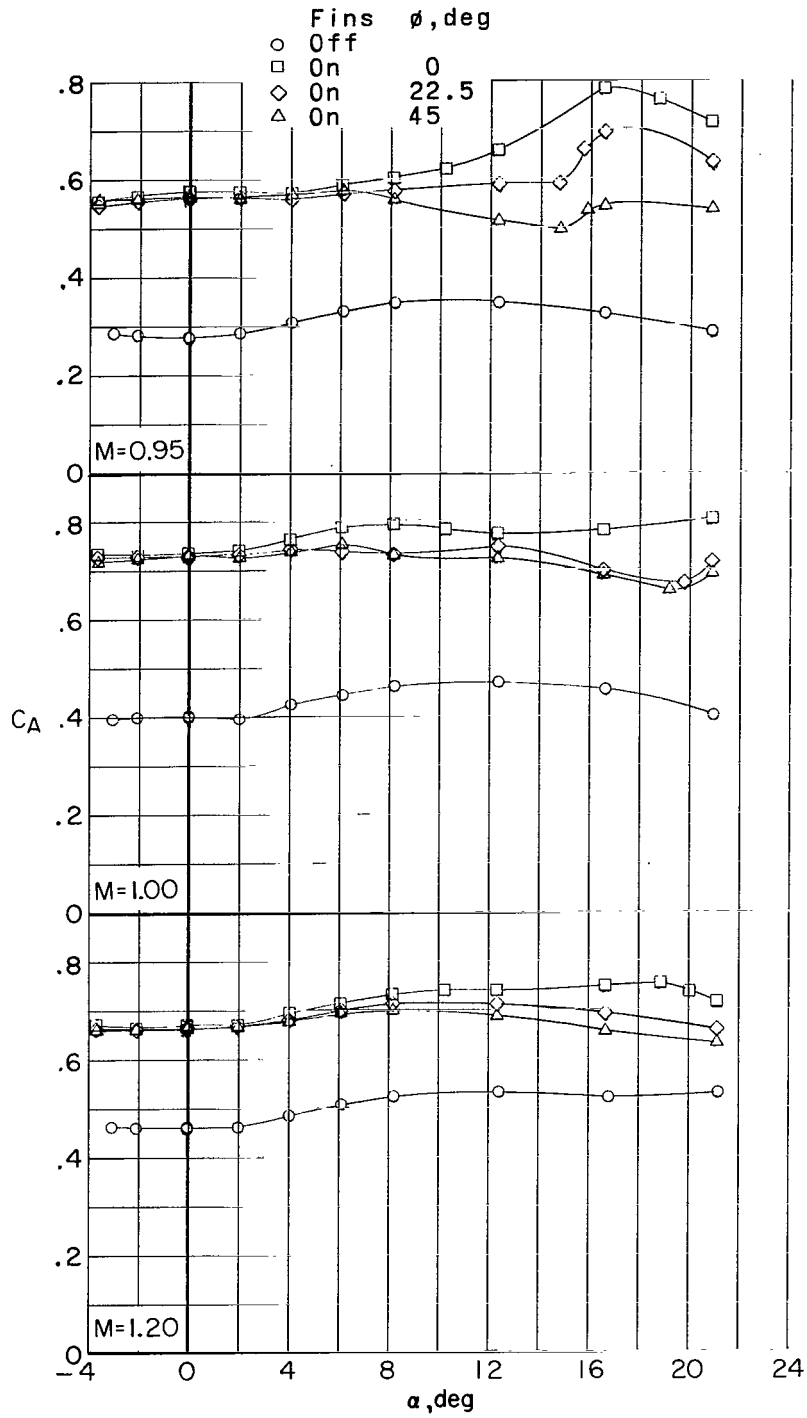

(a) Concluded.

Figure 8.- Continued.

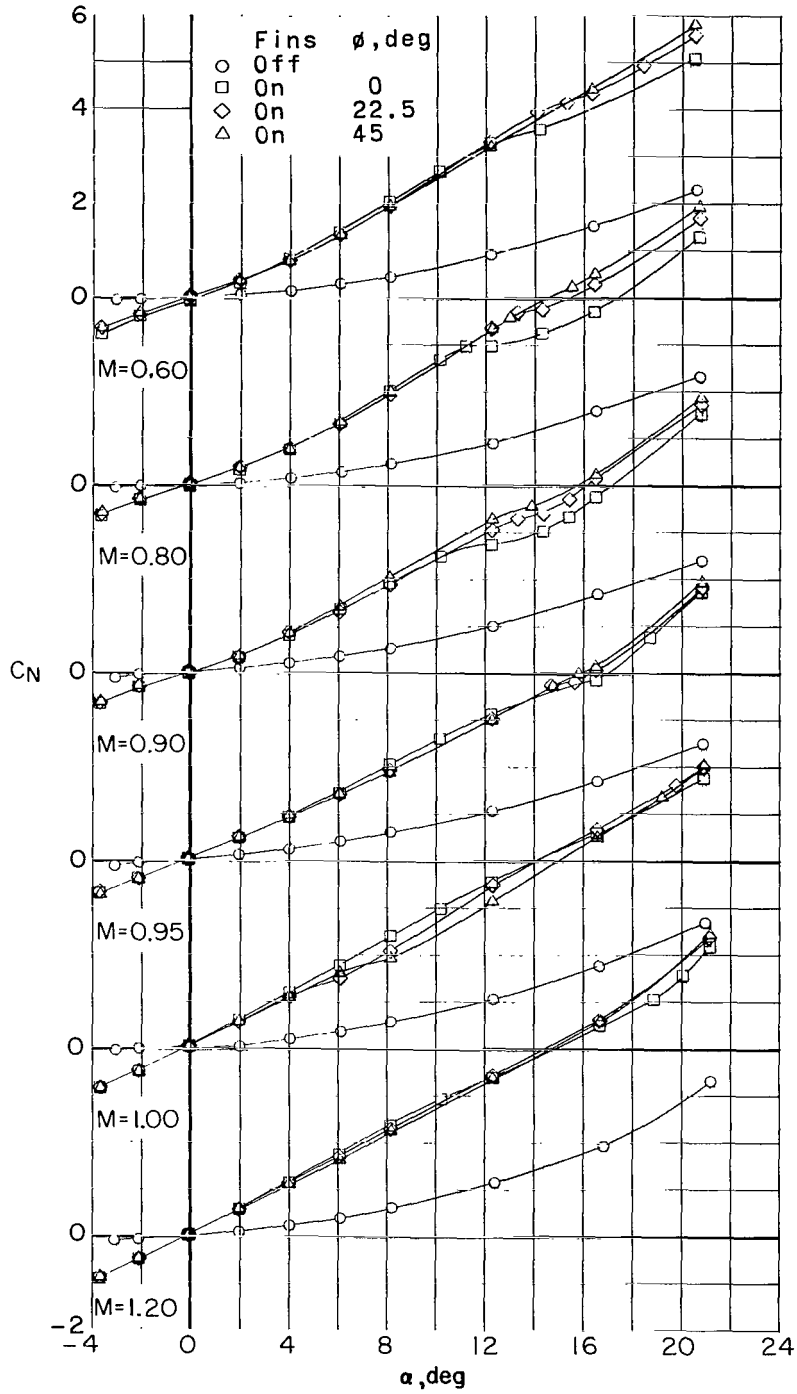

(b) Normal-force coefficient.

Figure 8.- Continued.

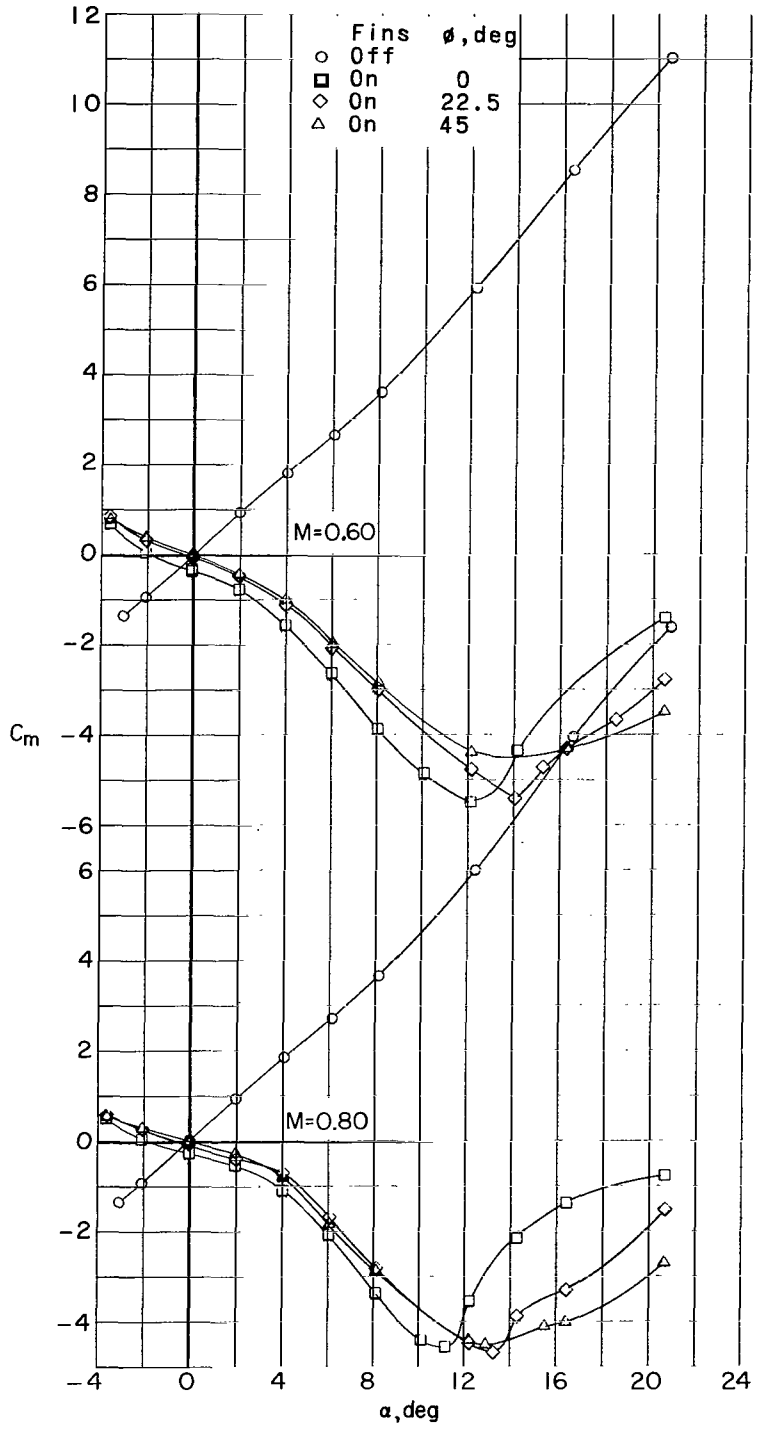

(c) Pitching-moment coefficient.

Figure 8.- Continued.

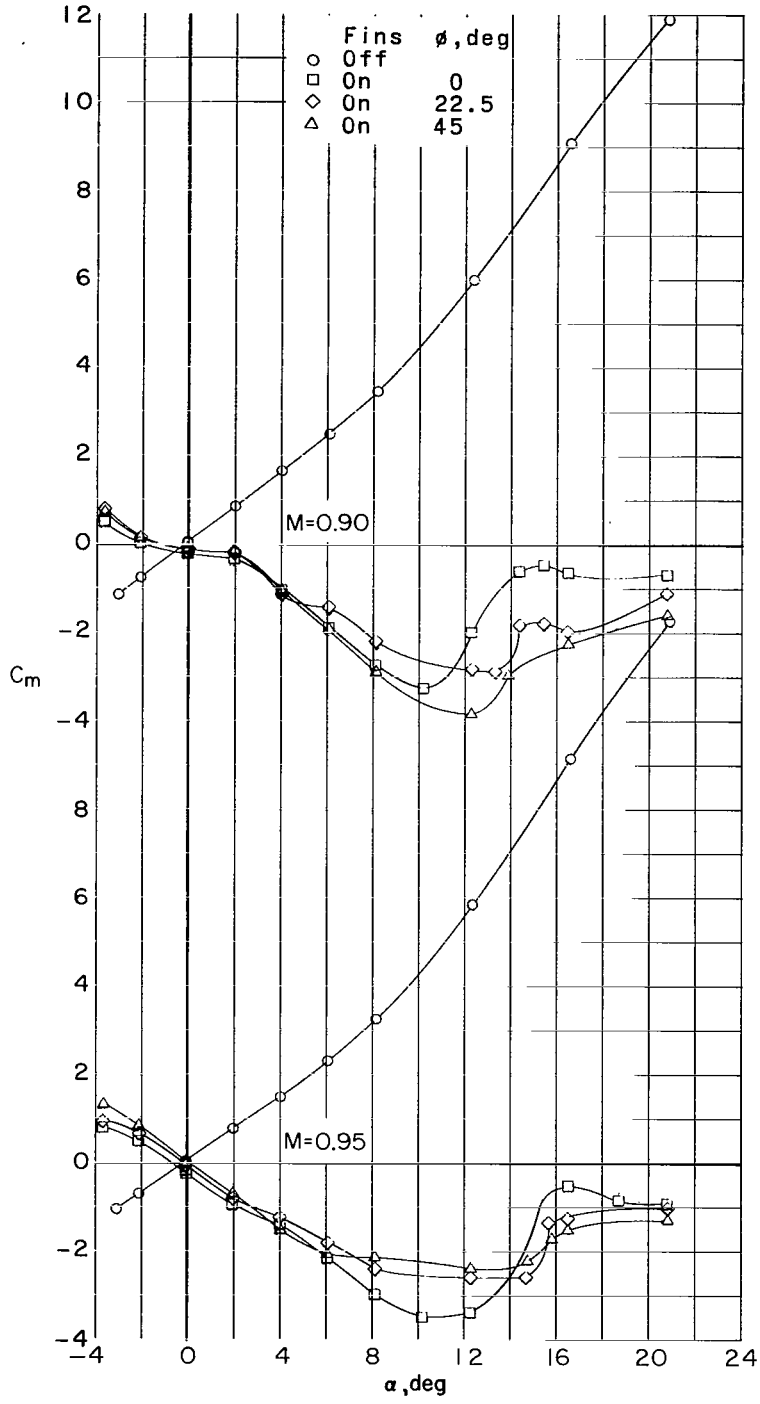

(c) Continued.

Figure 8.- Continued.

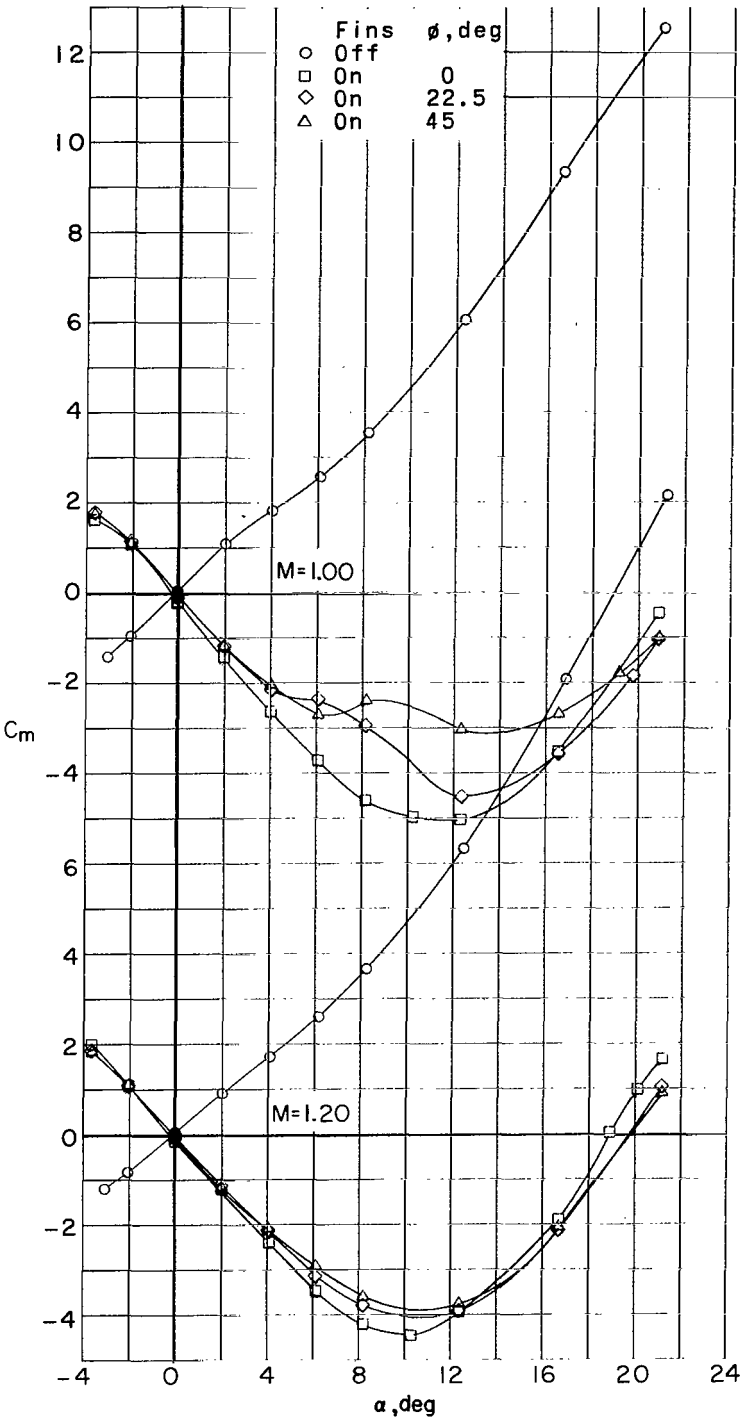

(c) Concluded.

Figure 8.- Continued.

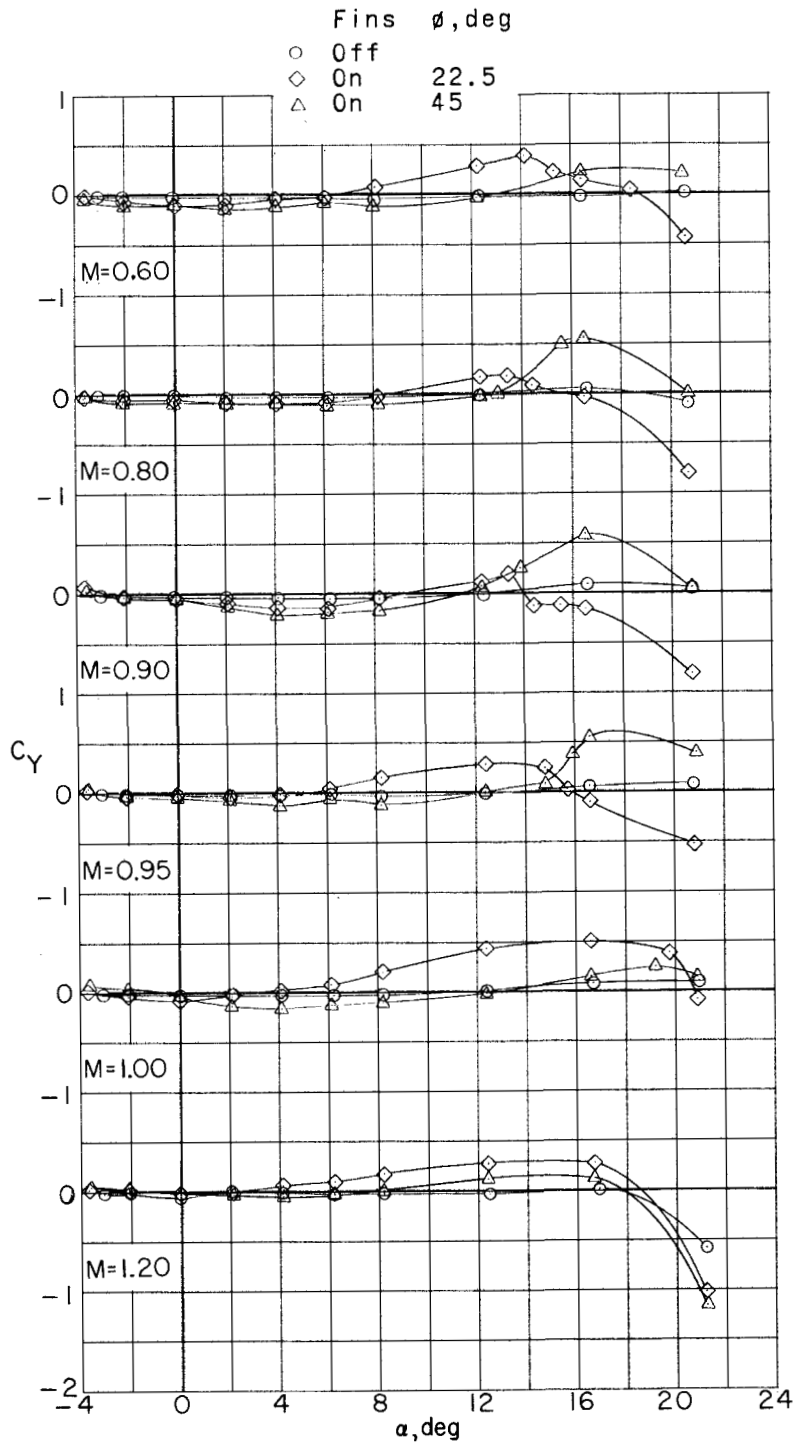

(d) Side-force coefficient.

Figure 8.- Continued.

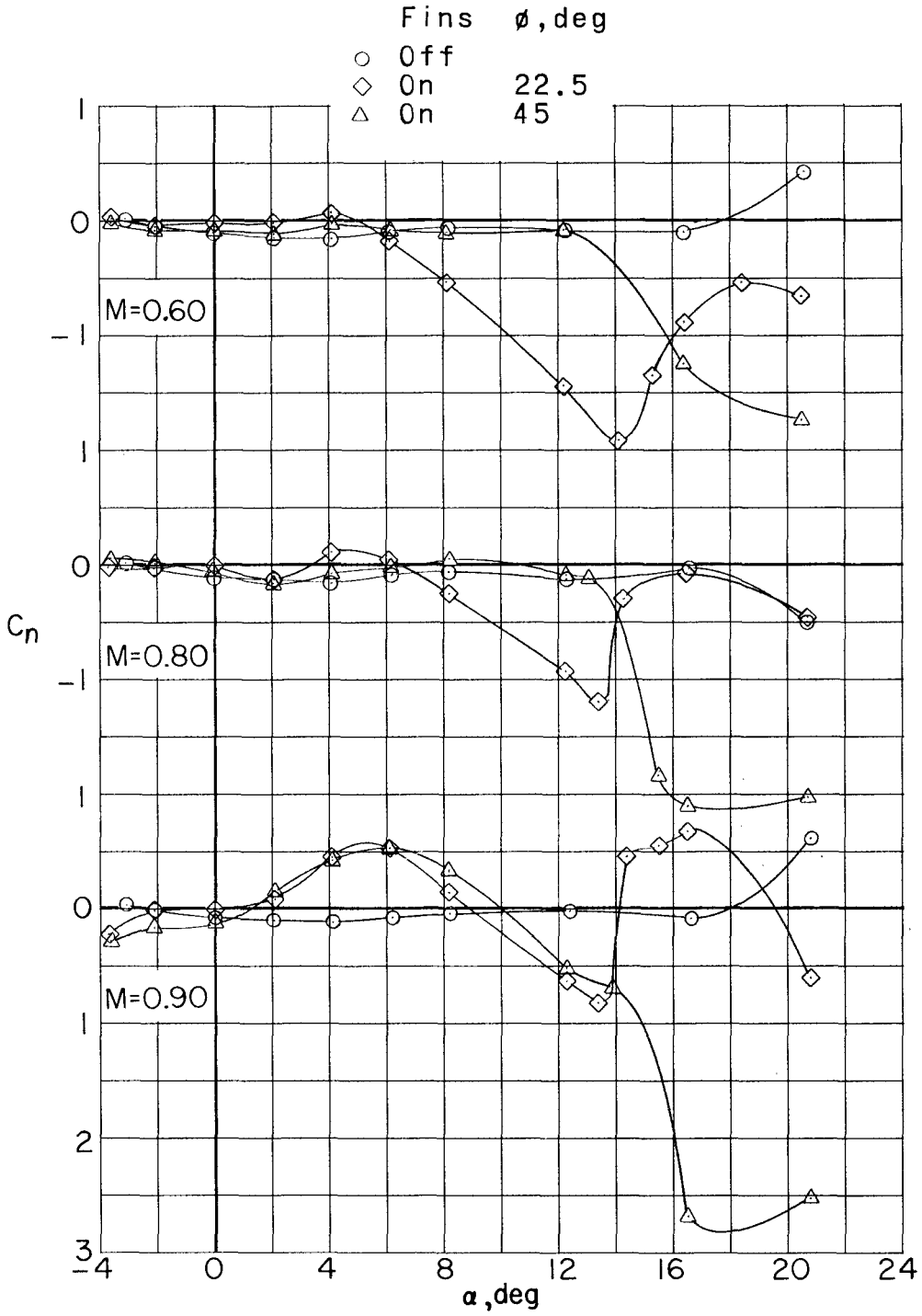

(e) Yawing-moment coefficient.

Figure 8.- Continued.

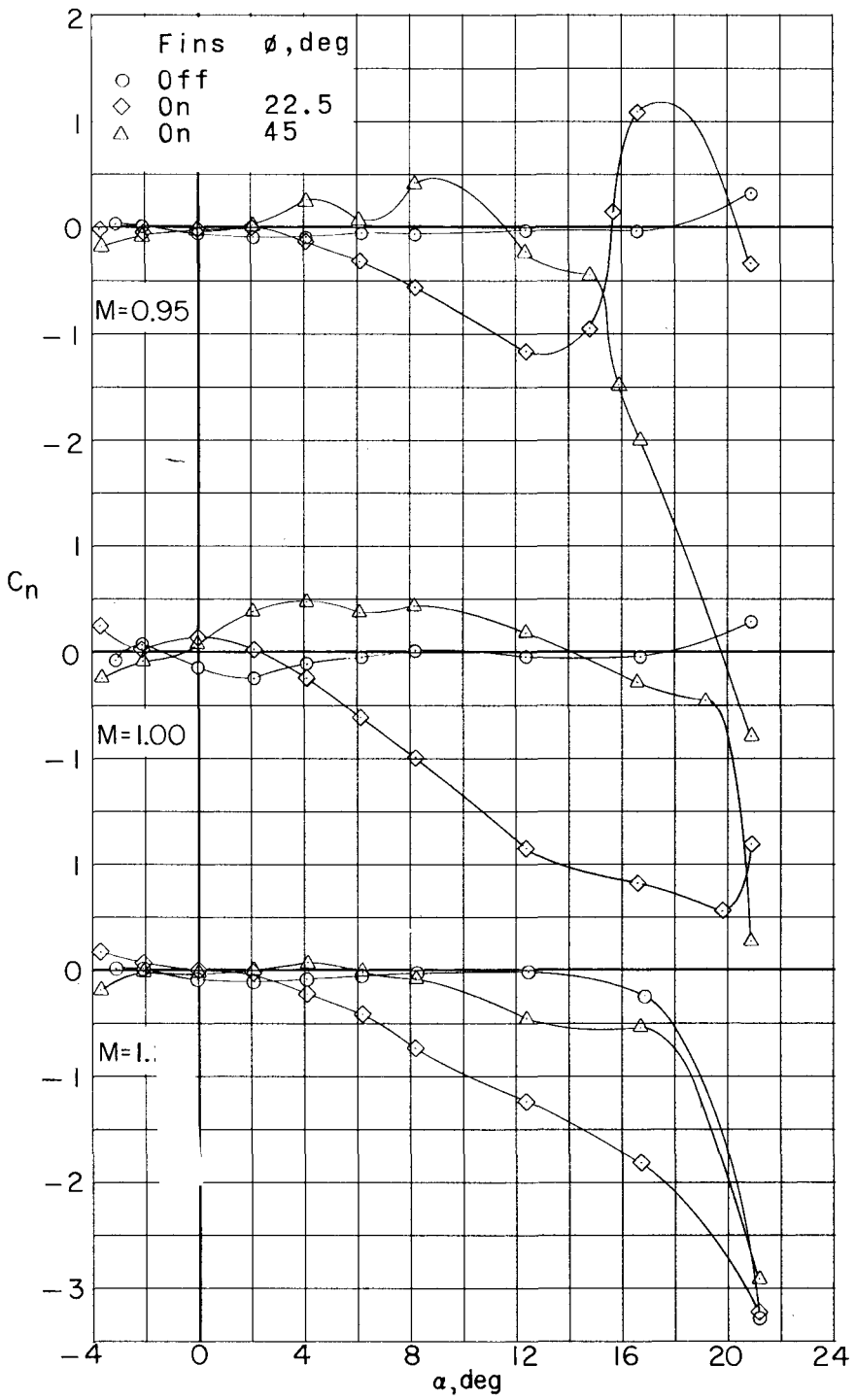

(e) Concluded.

Figure 8.- Continued.

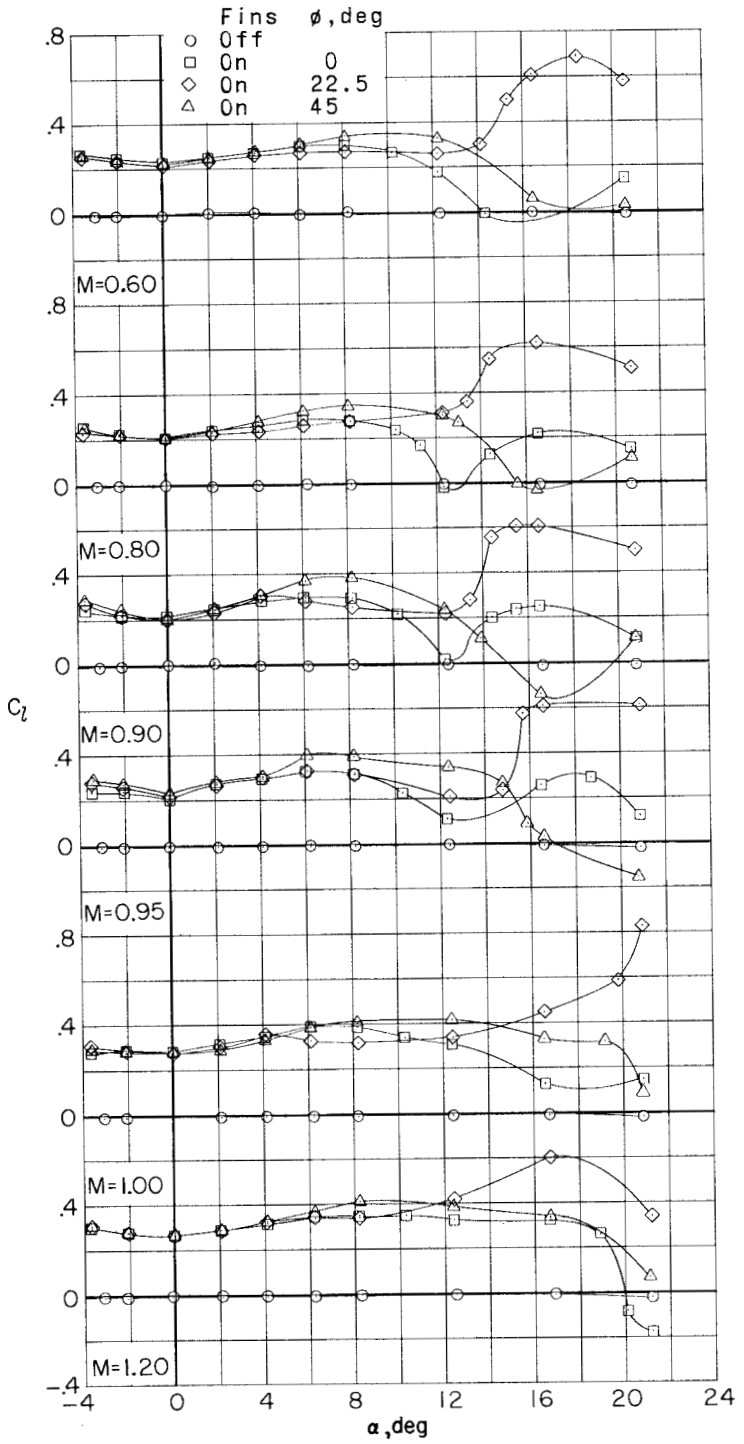

(f) Rolling-moment coefficient.

Figure 8.- Concluded.

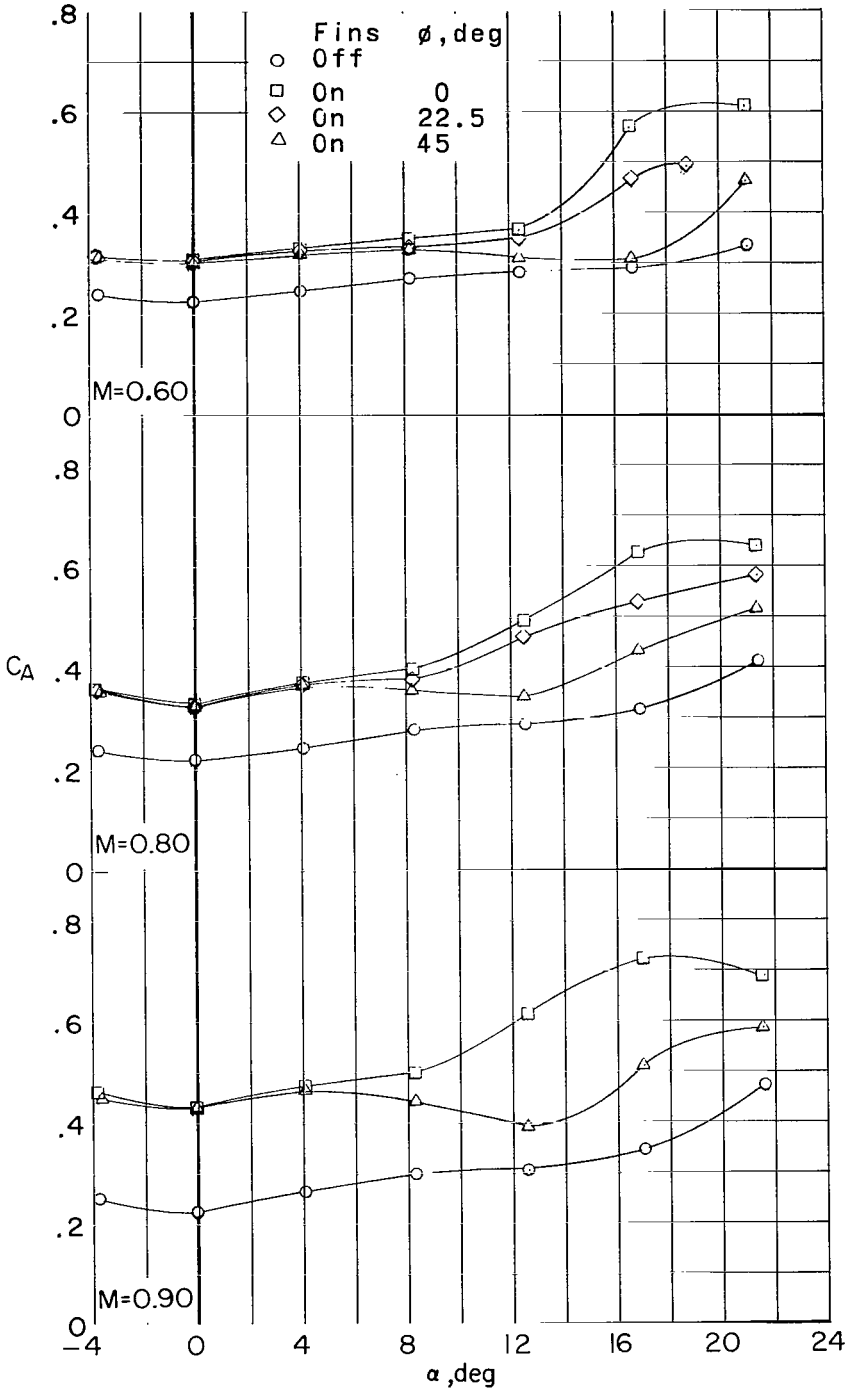

(a) Axial-force coefficient.

Figure 9.- Effect of roll angle on aerodynamic characteristics. Long model; $\delta_F = 0^0$.

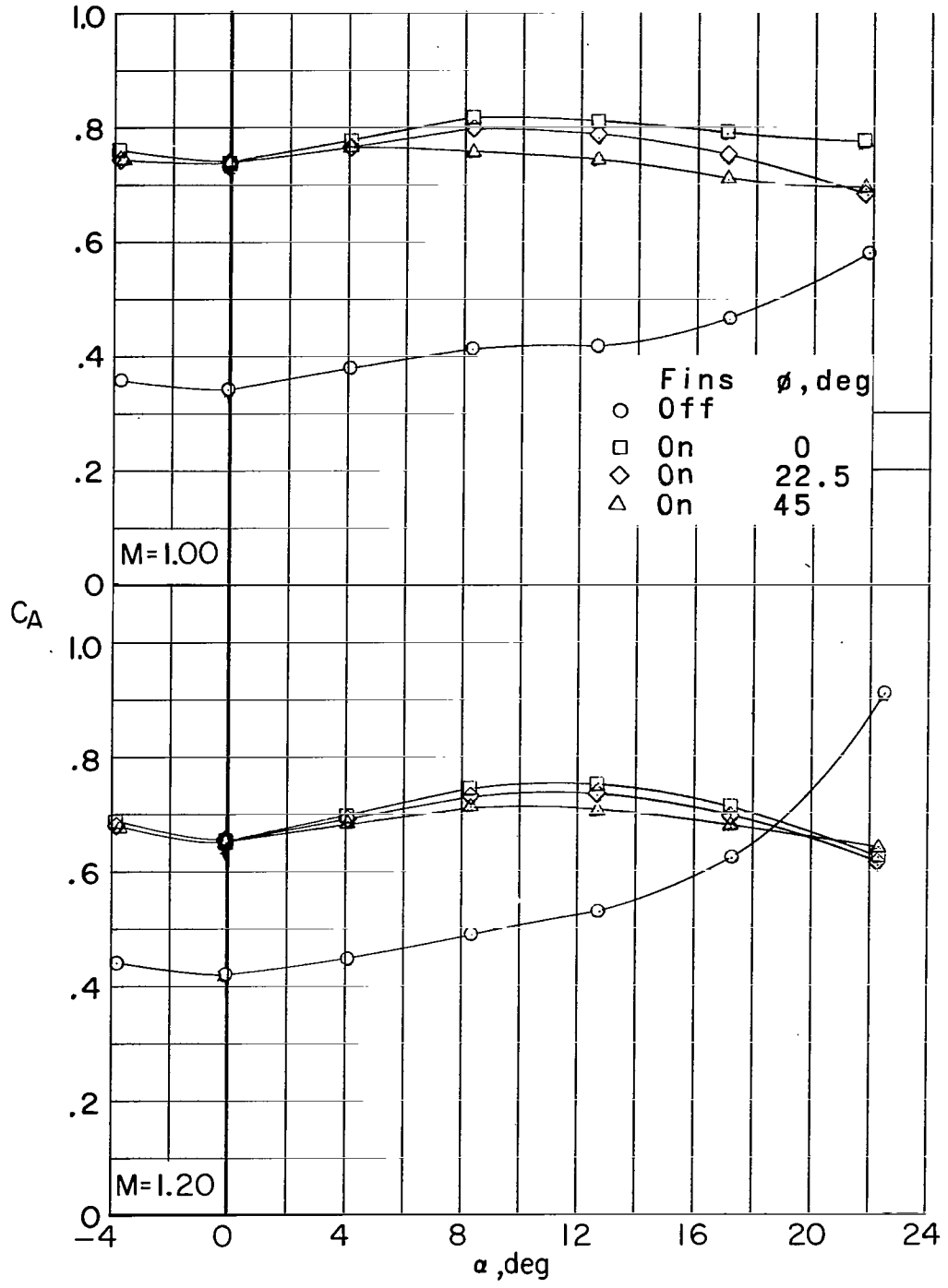

(a) Concluded.

Figure 9.- Continued.

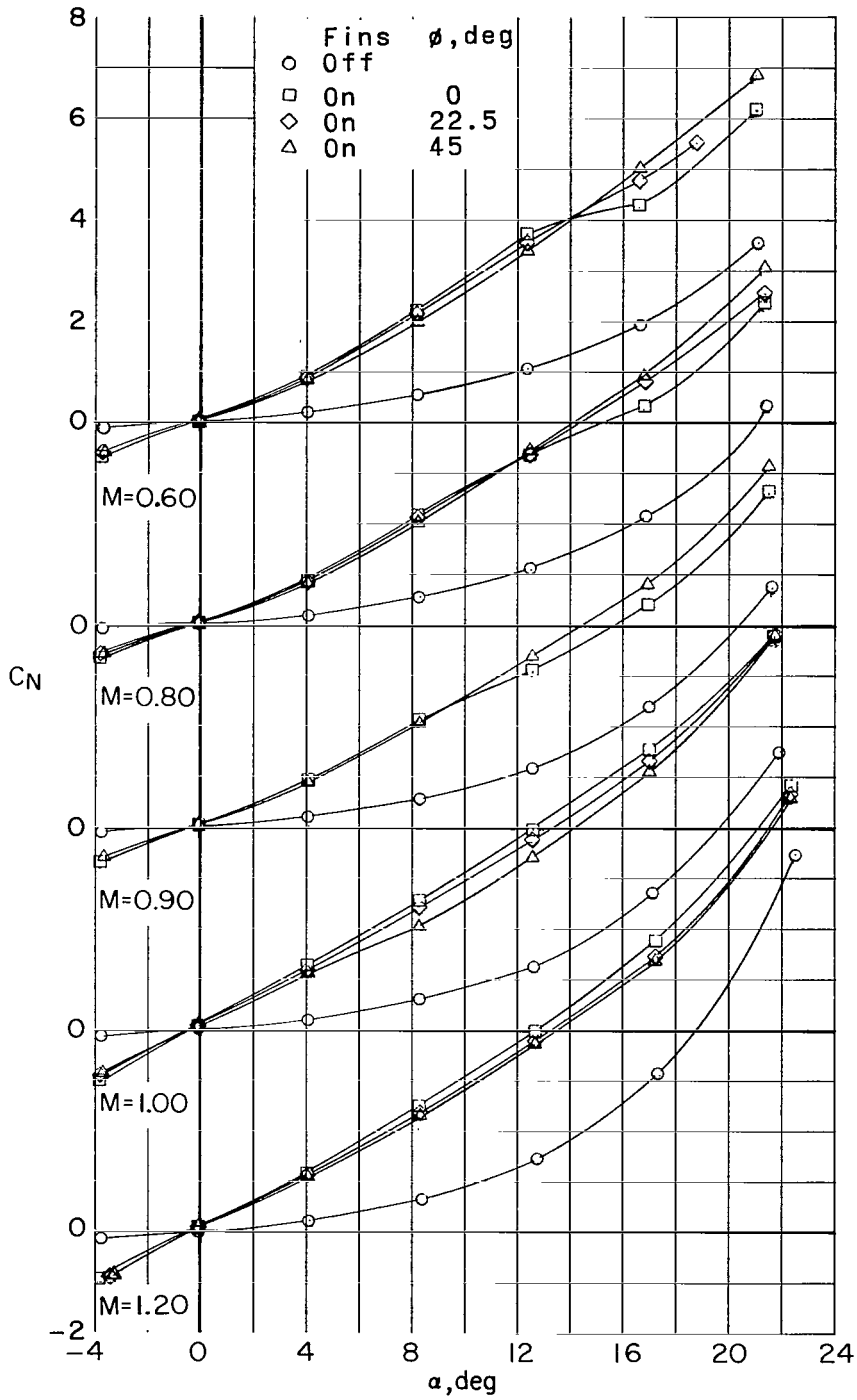

(b) Normal-force coefficient.

Figure 9.- Continued.

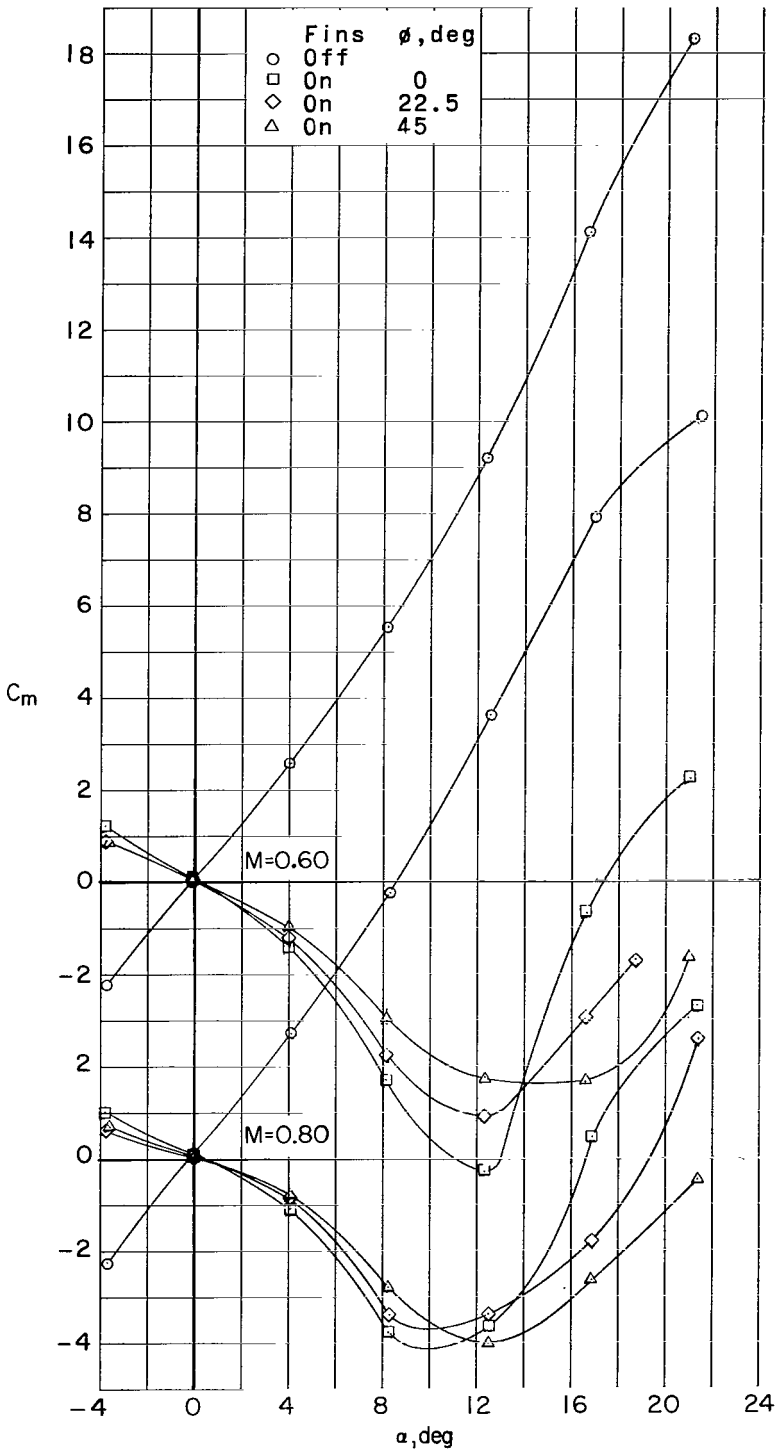

(c) Pitching-moment coefficient.

Figure 9.- Continued.

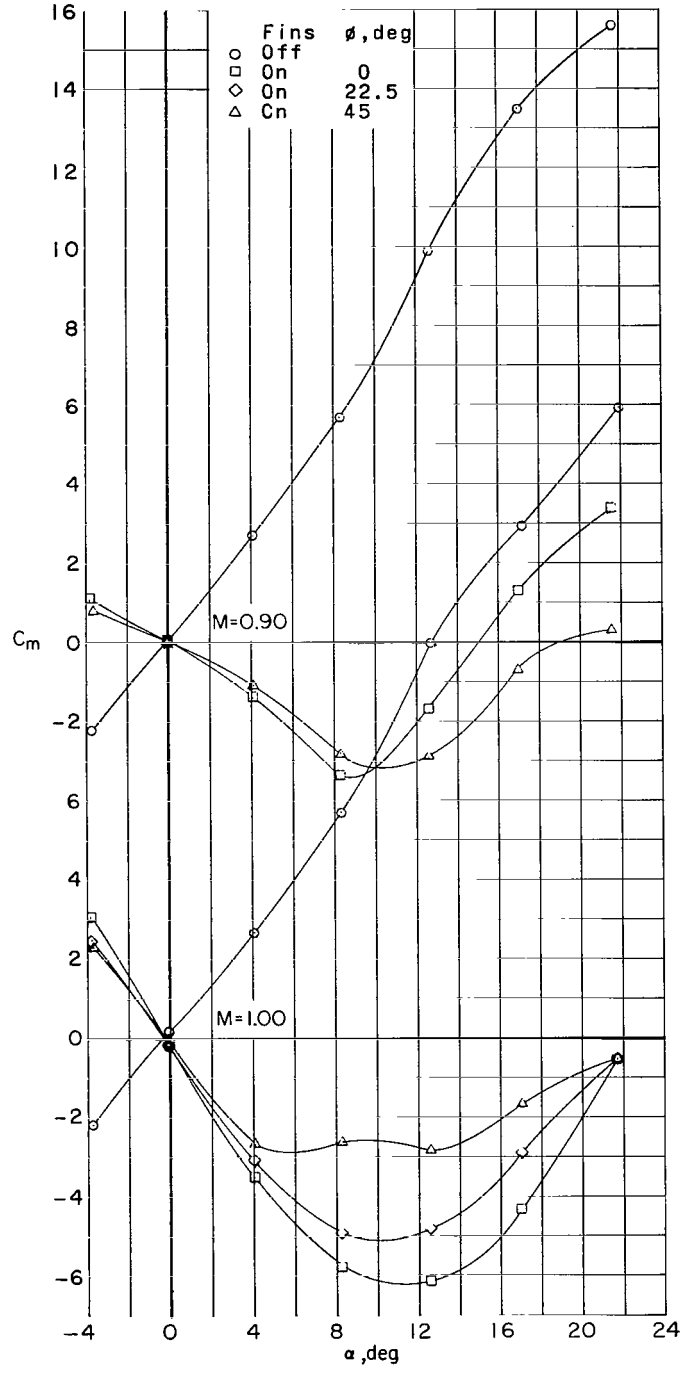

(c) Continued.

Figure 9.- Continued.

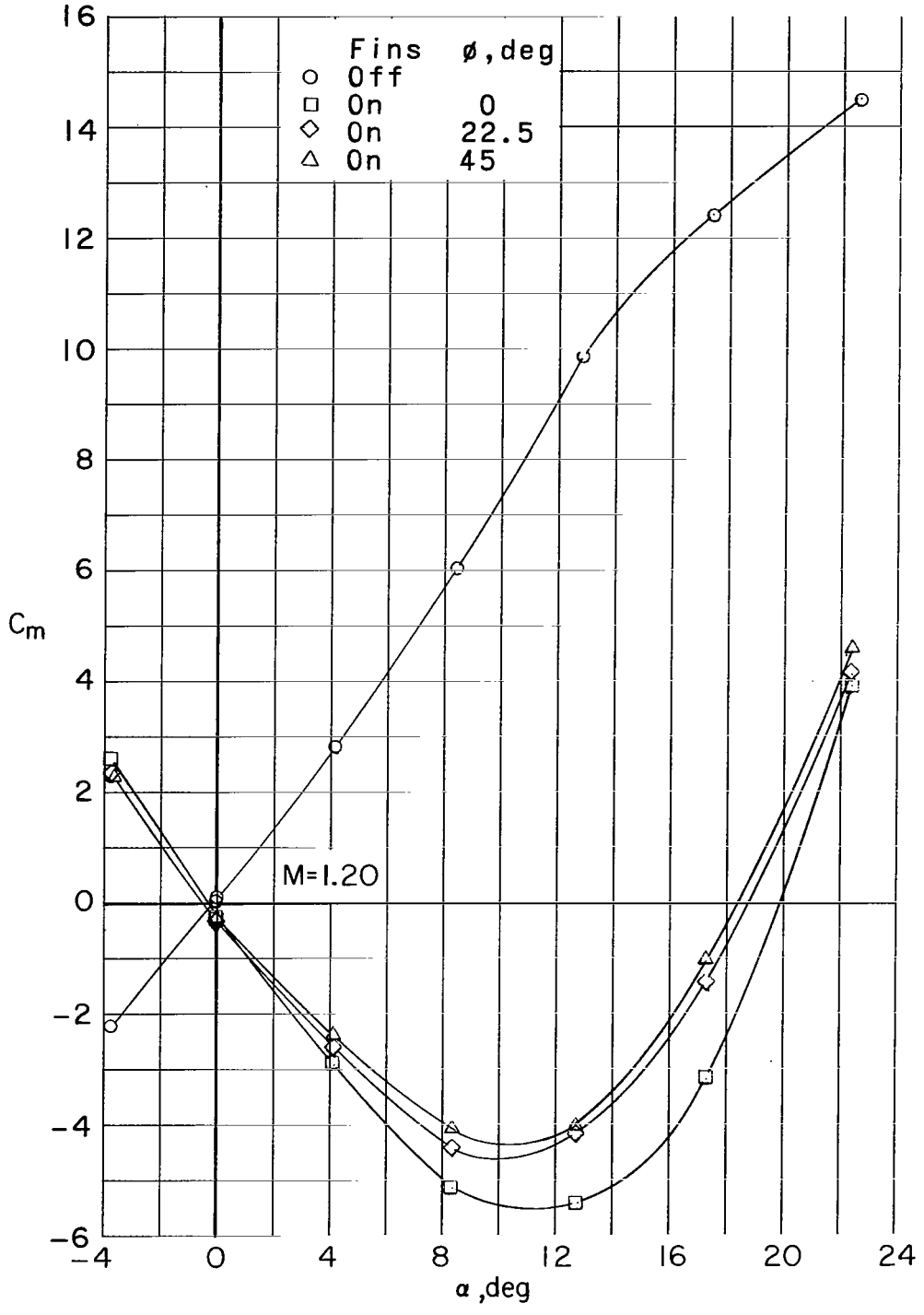

(c) Concluded.

Figure 9.- Continued.

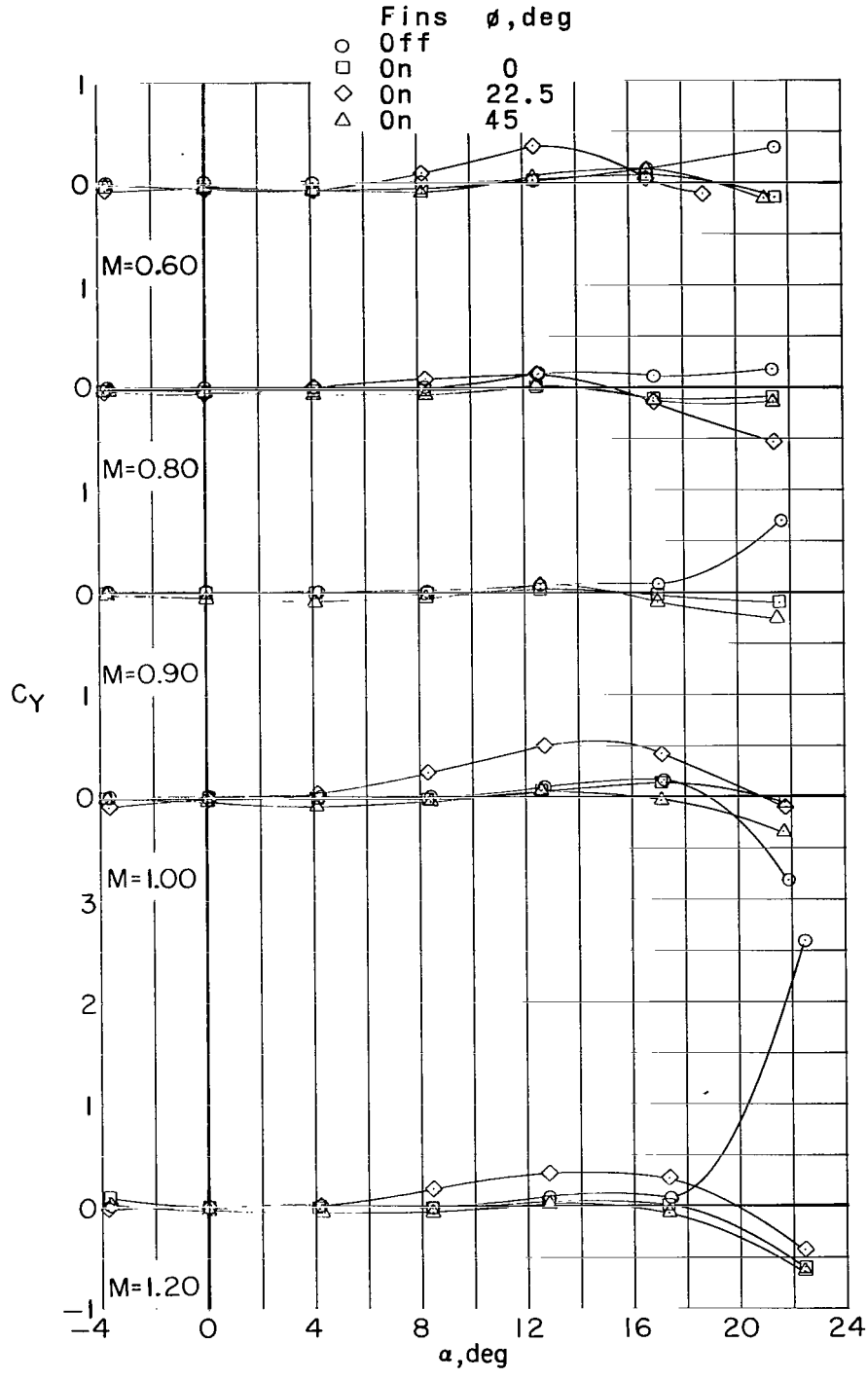

(d) Side-force coefficient.

Figure 9.- Continued.

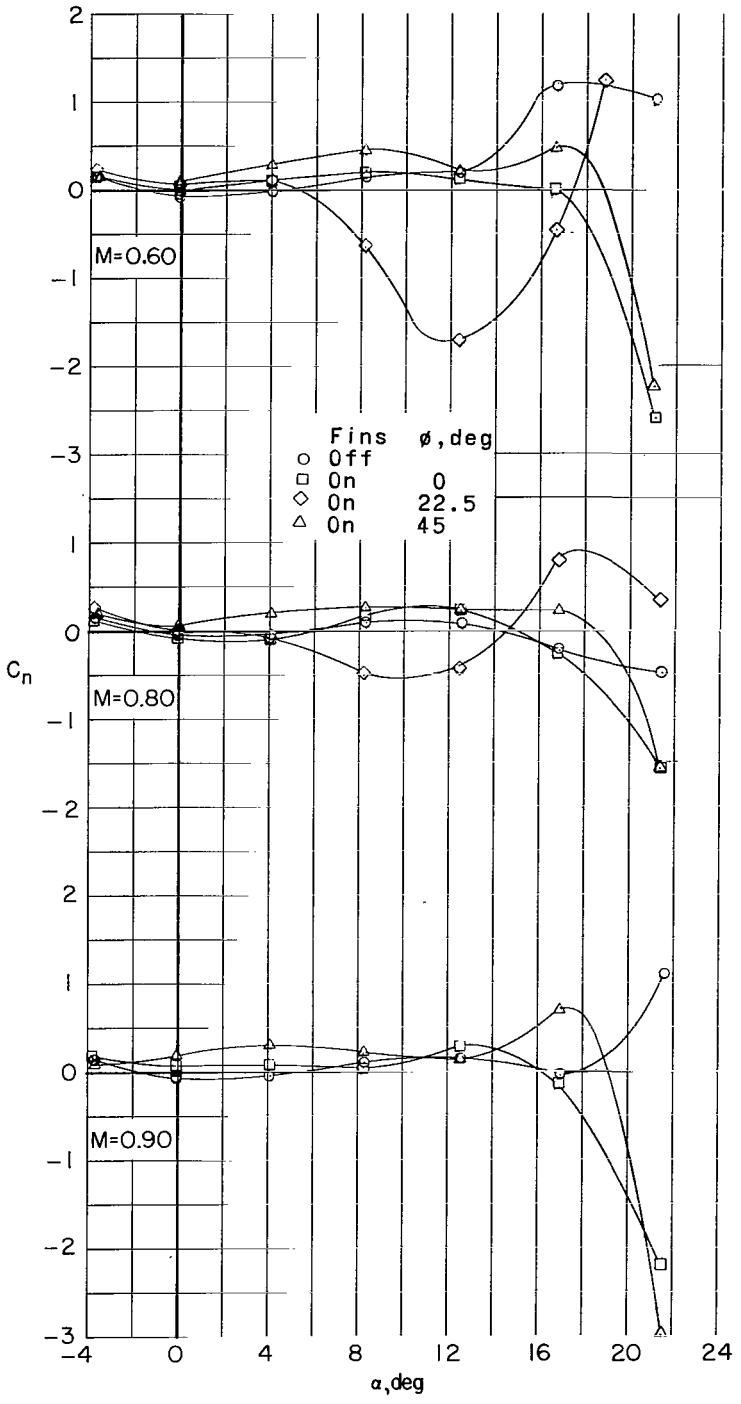

(e) Yawing-moment coefficient.

Figure 9.- Continued.

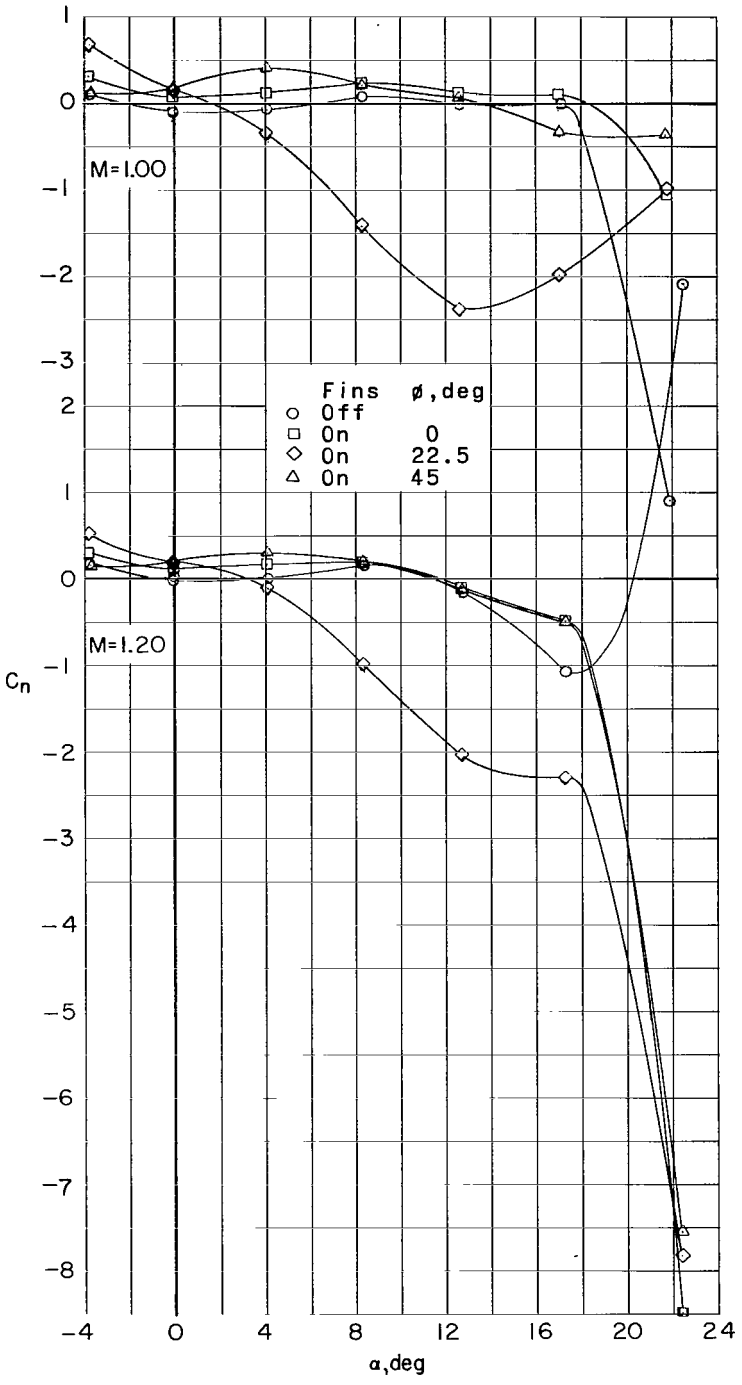

(e) Concluded.

Figure 9.- Continued.

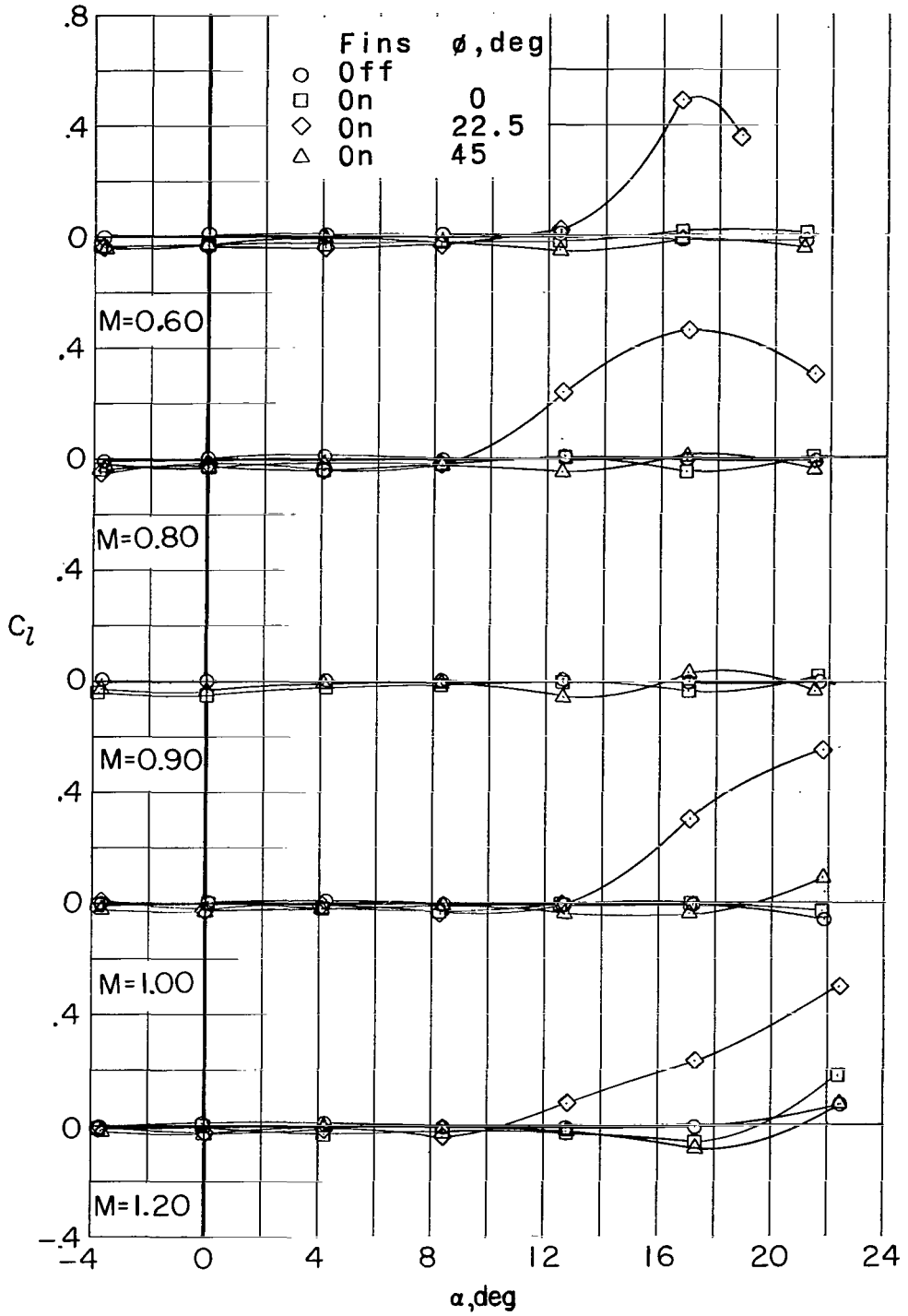

(f) Rolling-moment coefficient.

Figure 9.- Concluded.

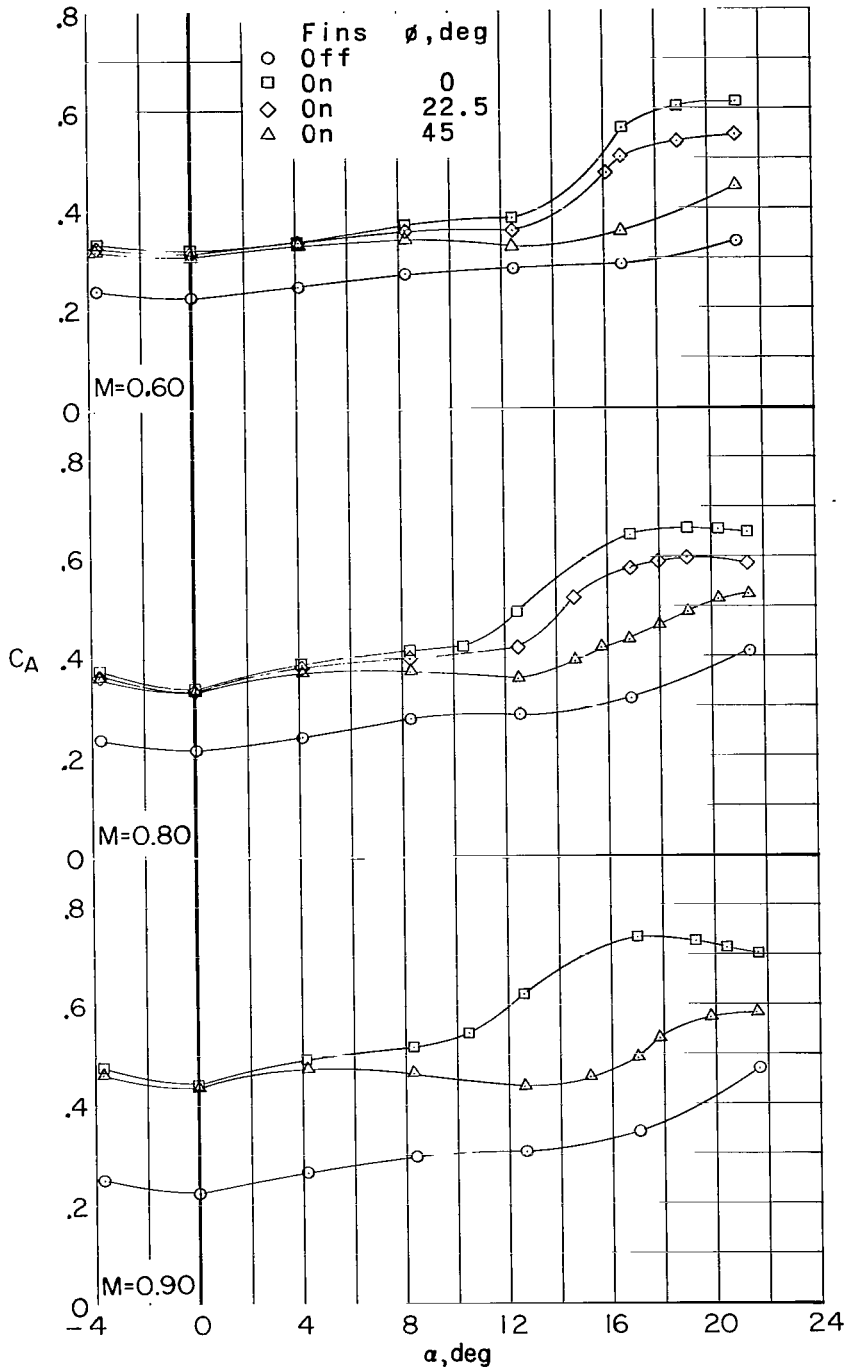

(a) Axial-force coefficient.

Figure 10.- Effect of roll angle on aerodynamic characteristics. Long model; $\delta_F = 2^o$.

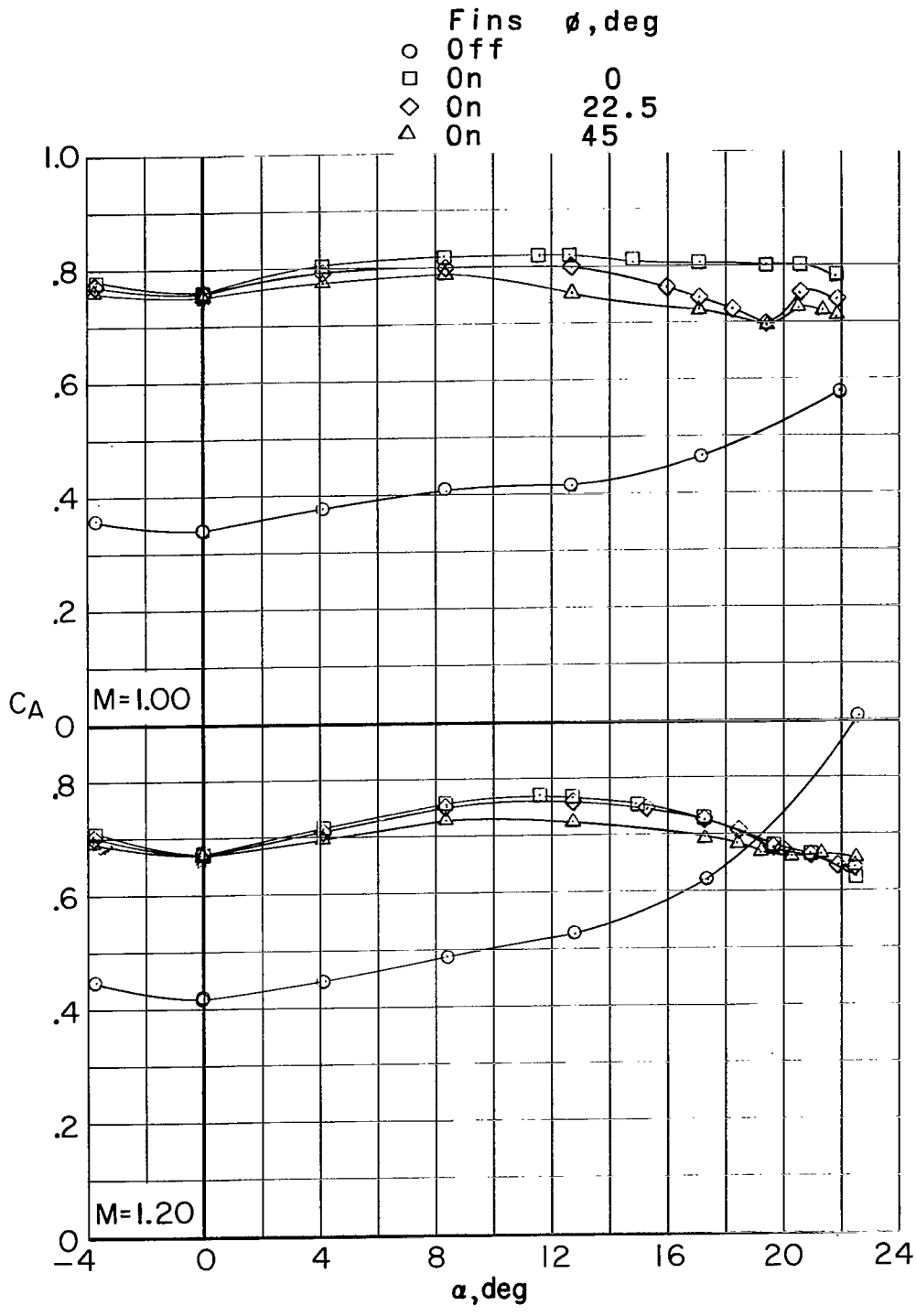

(a) Concluded.

Figure 10.- Continued.

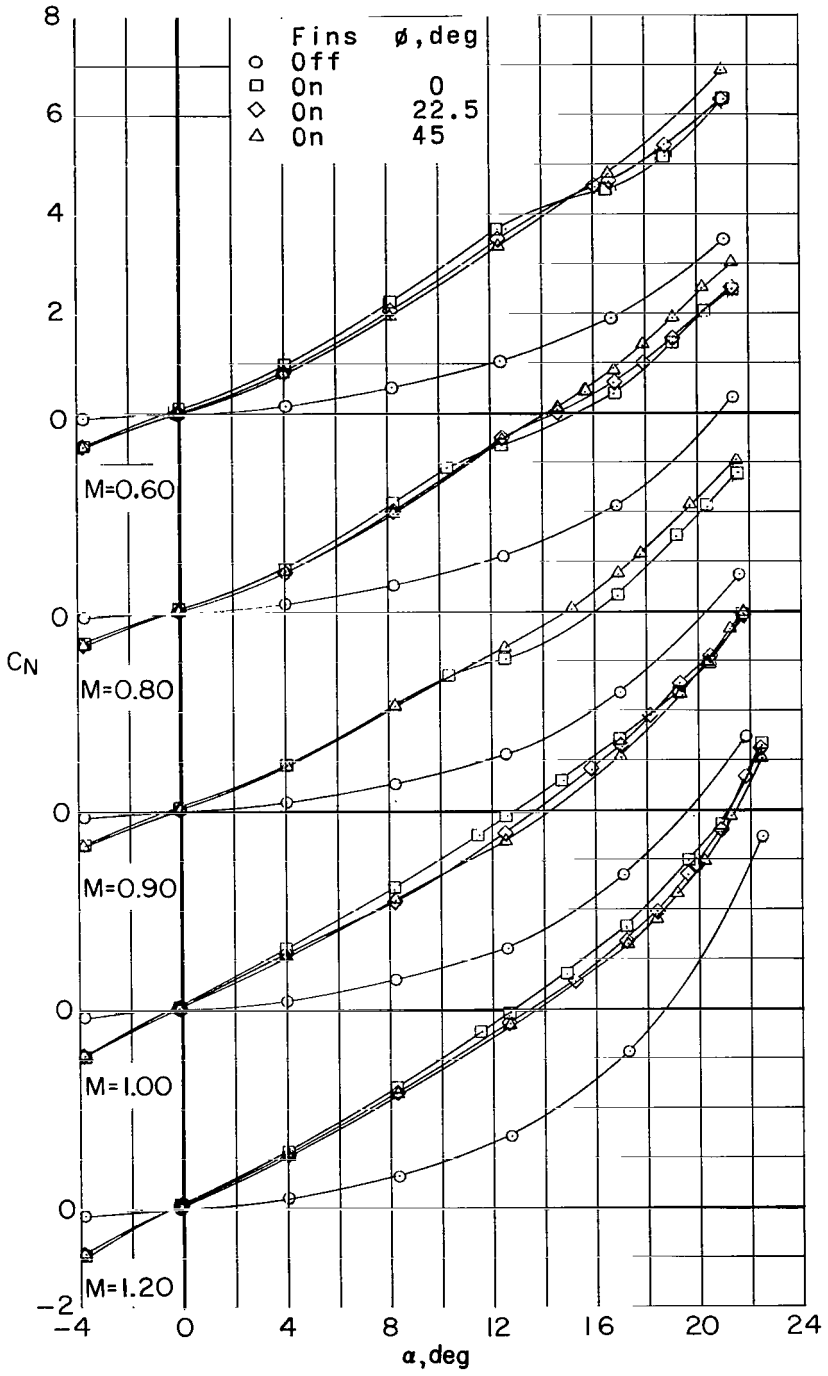

(b) Normal-force coefficient.

Figure 10.- Continued.

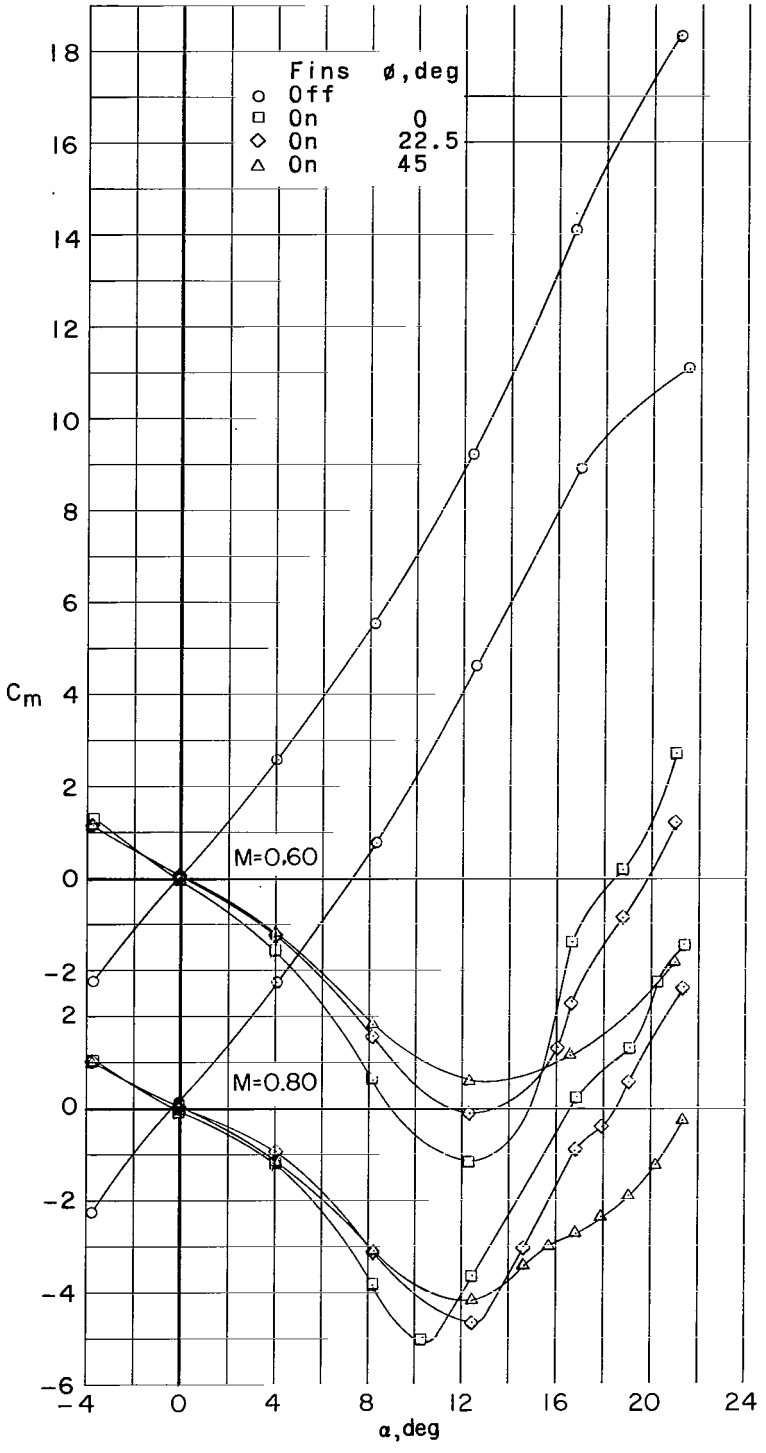

(c) Pitching-moment coefficient.

Figure 10.- Continued.

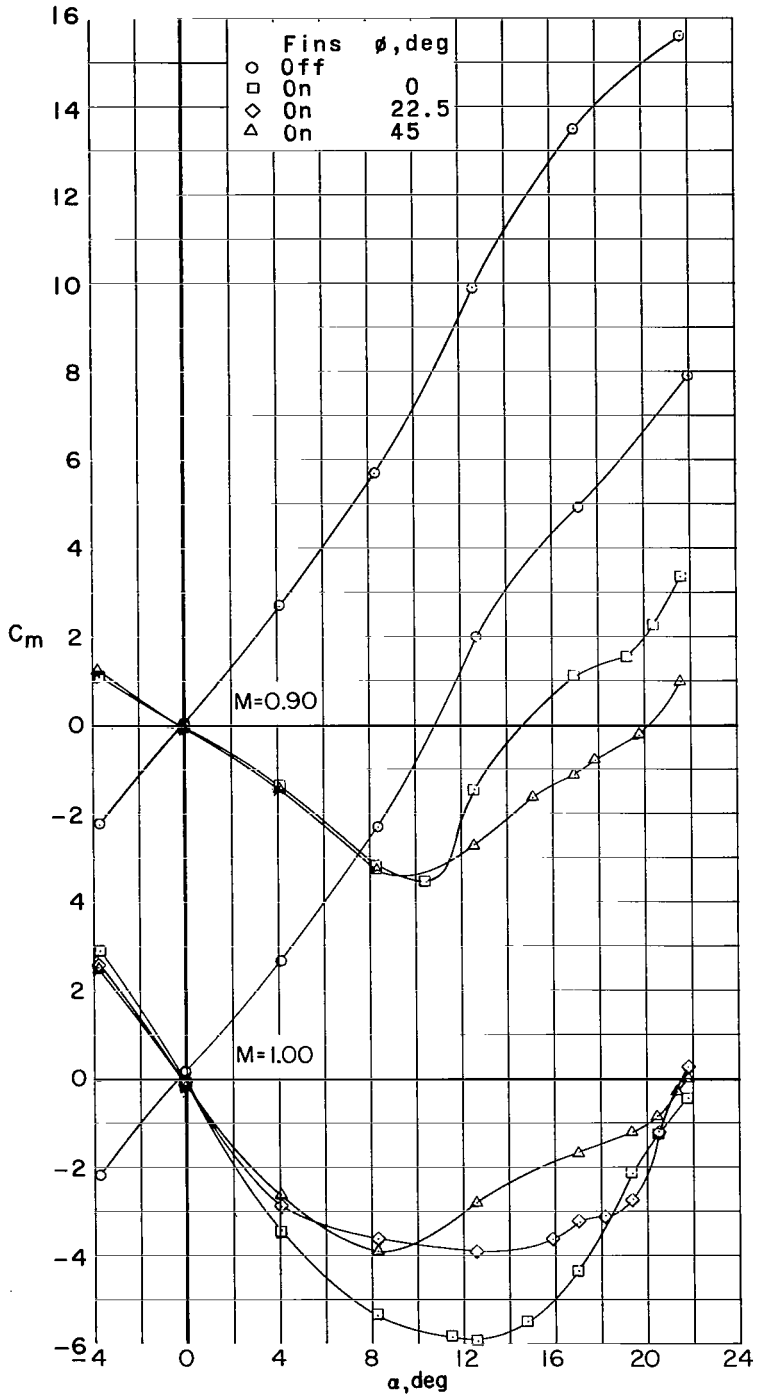

(c) Continued.

Figure 10.- Continued.

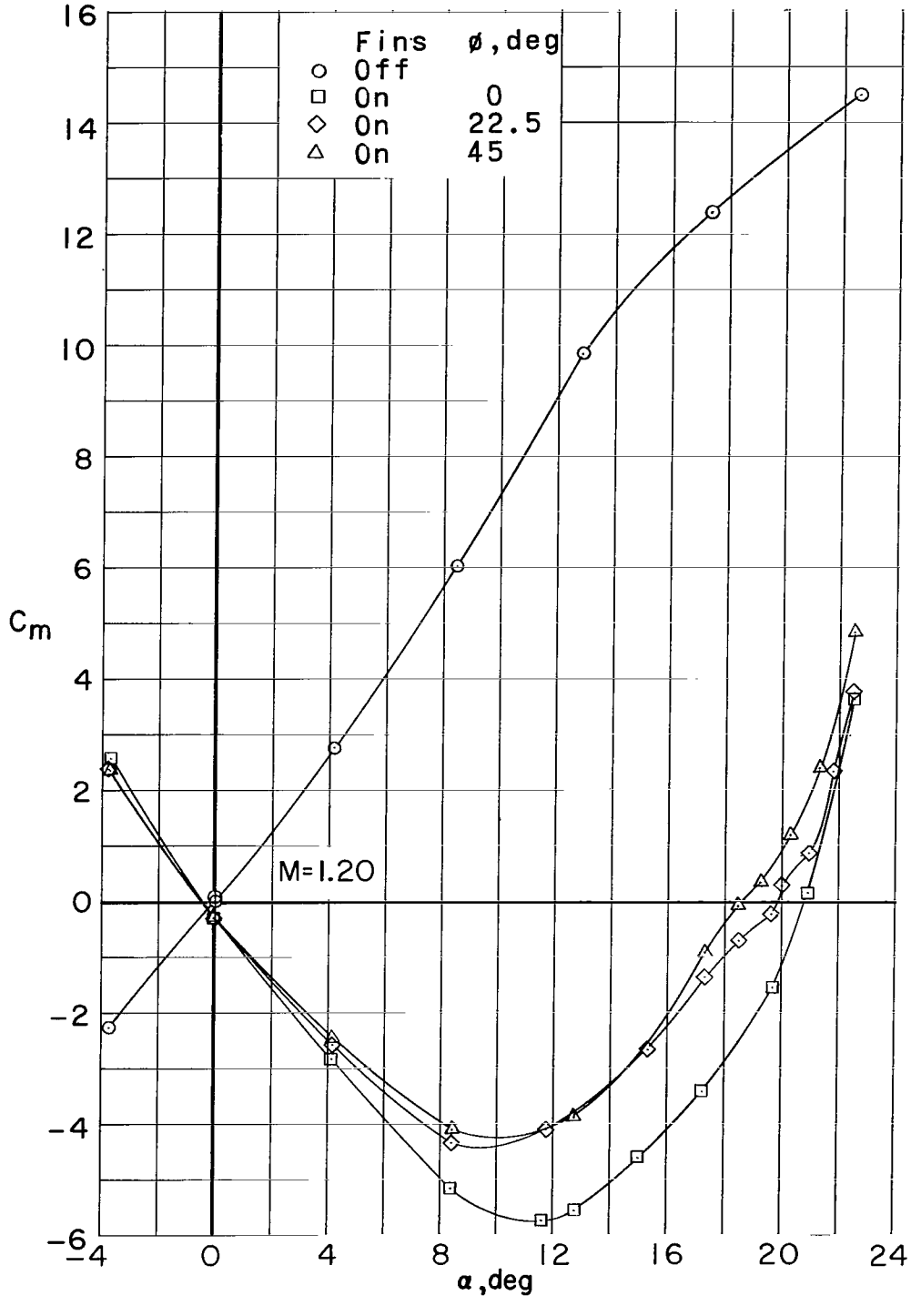

(c) Concluded.

Figure 10.- Continued.

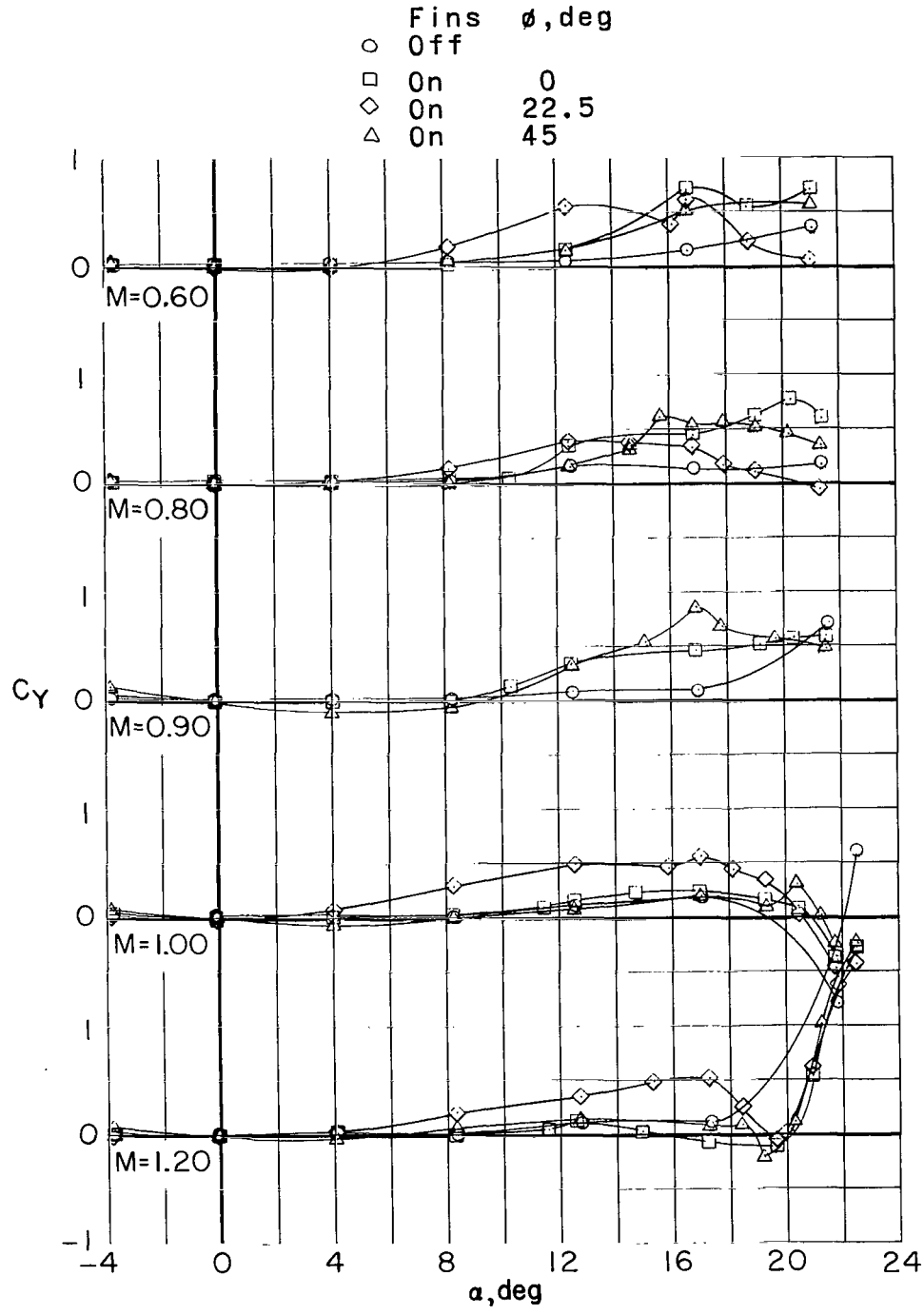

(d) Side-force coefficient.

Figure 10.- Continued.

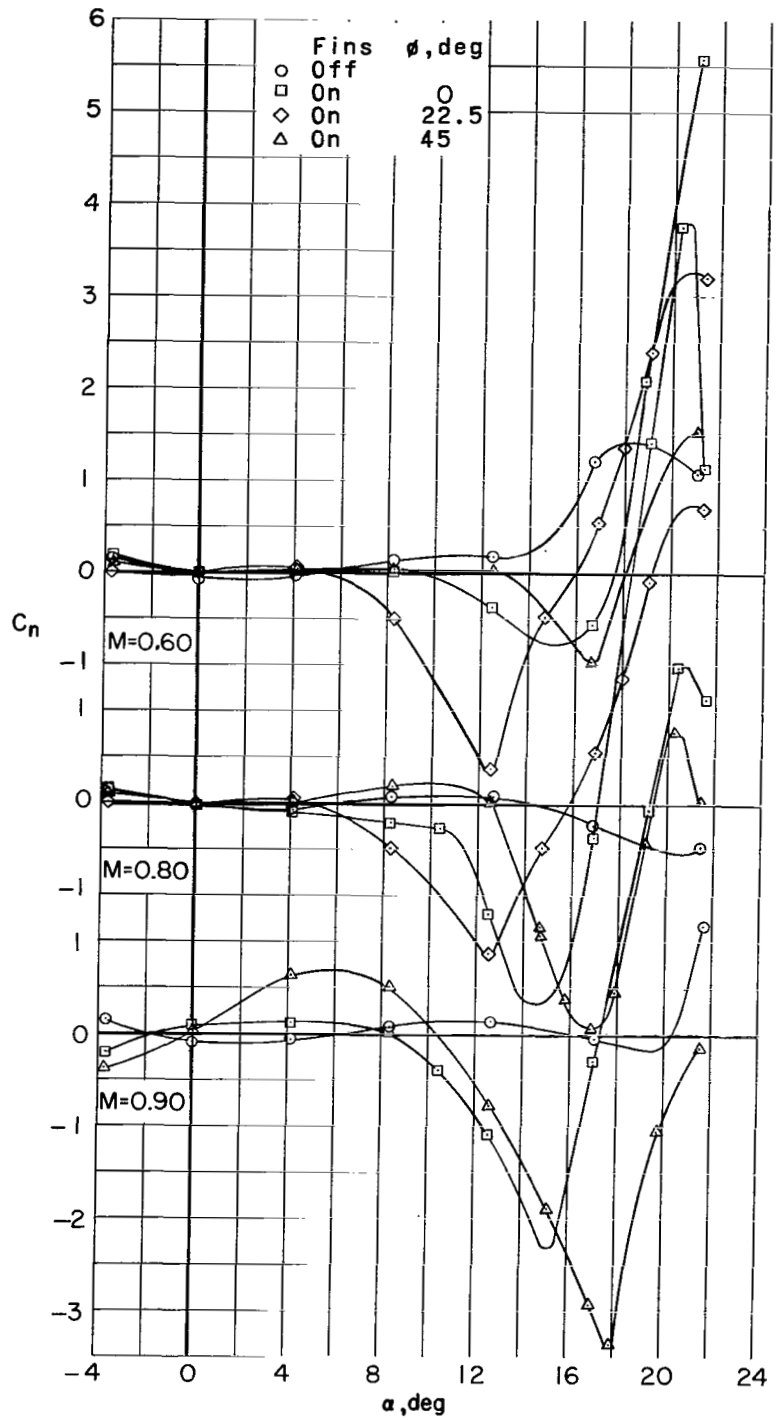

(e) Yawing-moment coefficient.

Figure 10.- Continued.

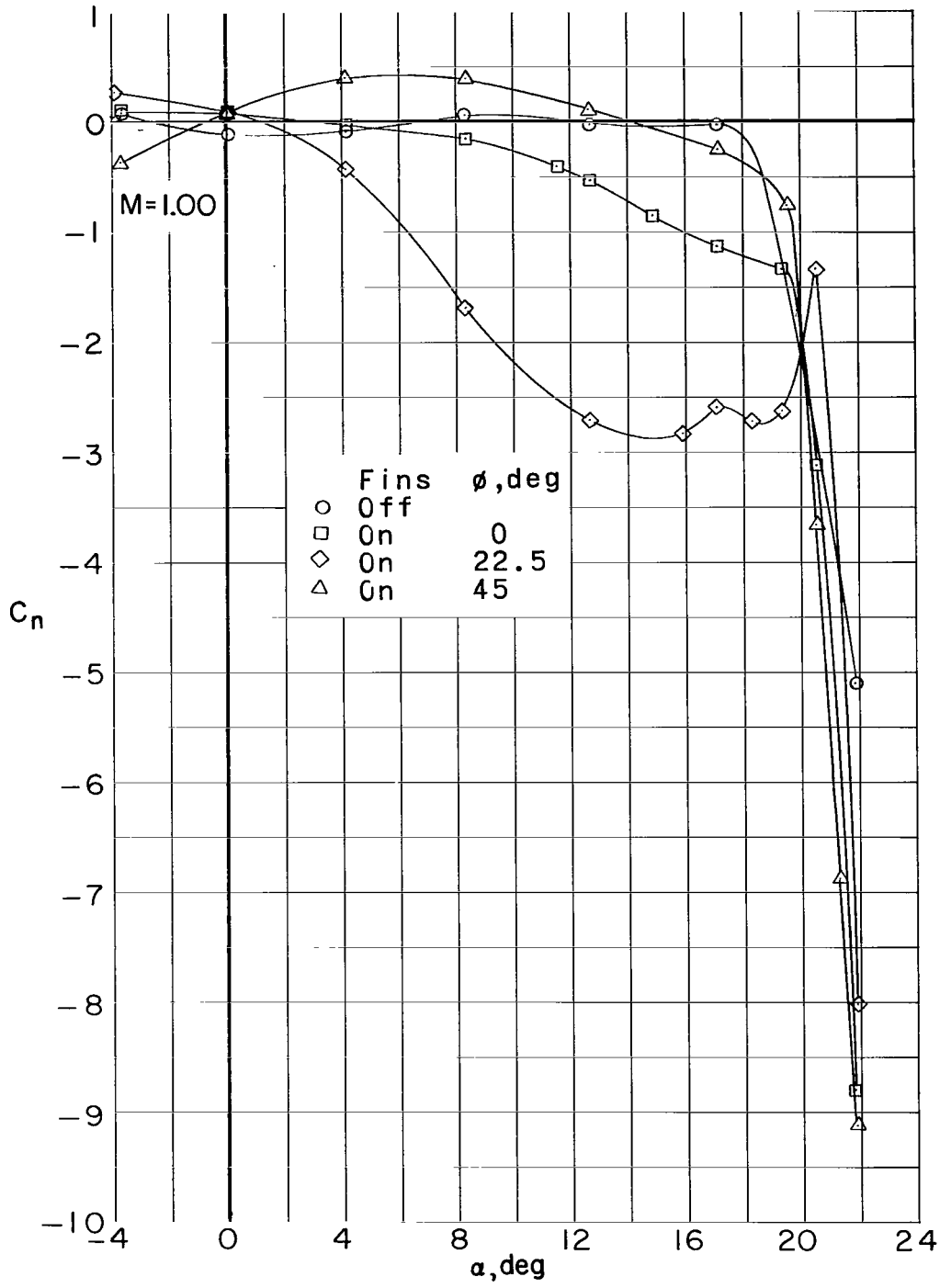

(e) Continued.

Figure 10.- Continued.

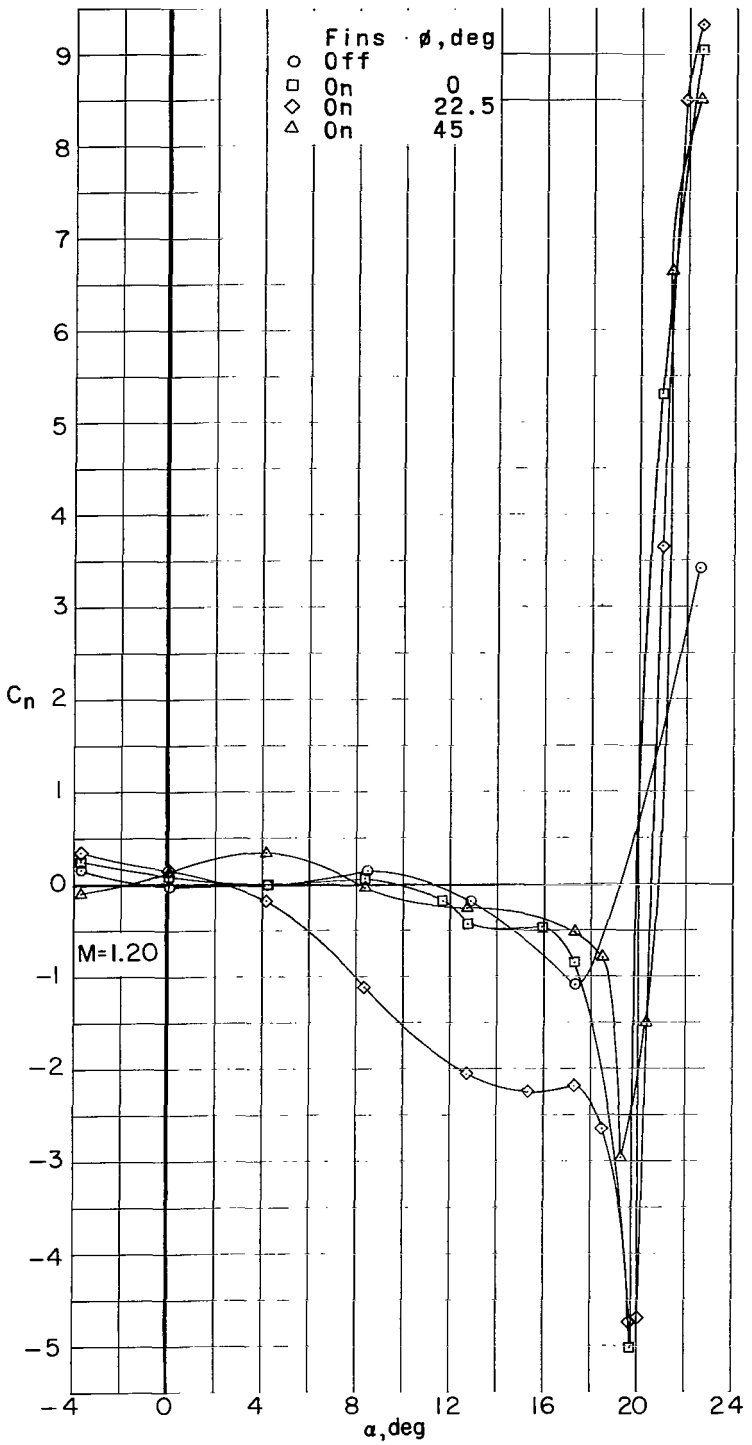

(e) Concluded.

Figure 10.- Continued.

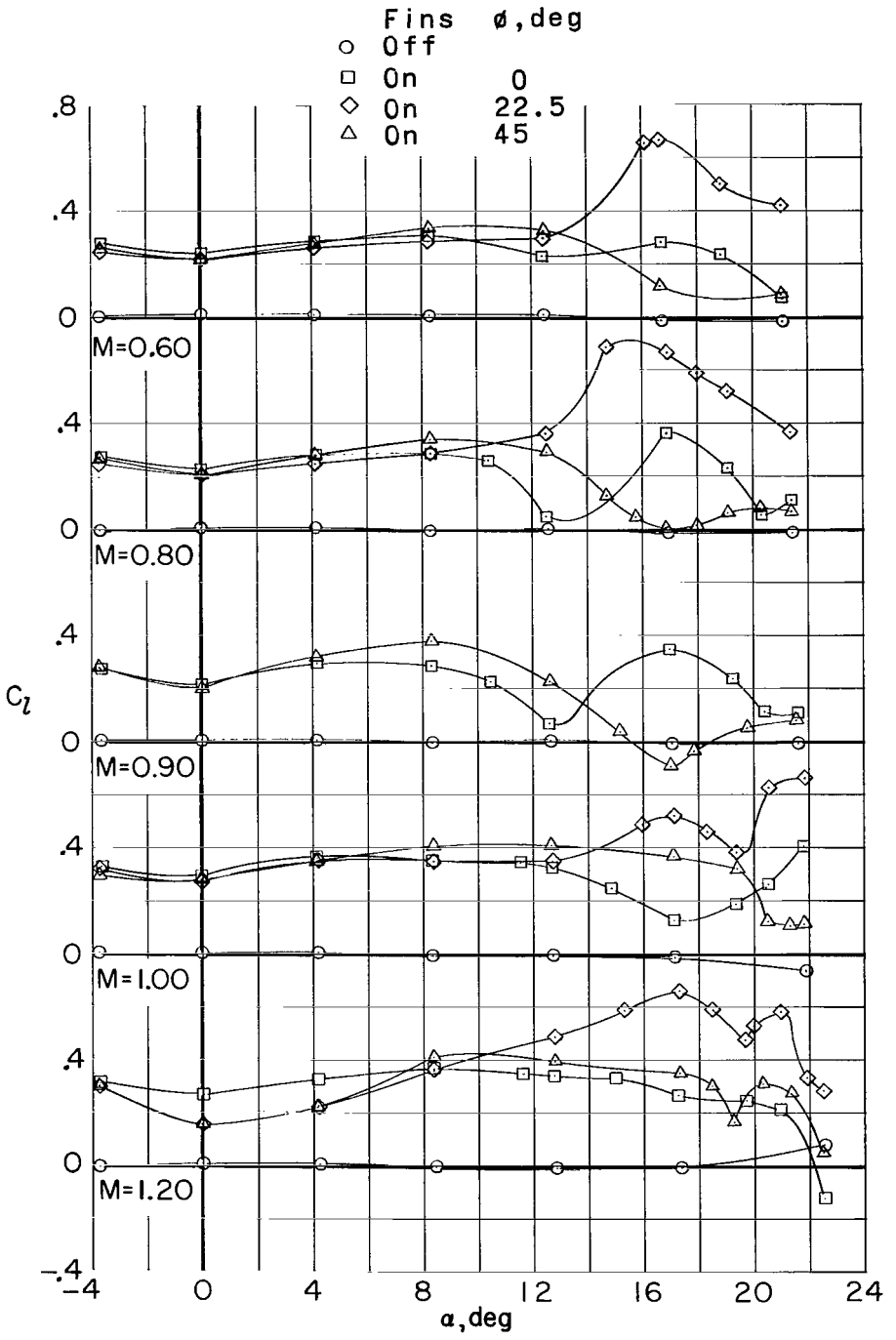

(f) Rolling-moment coefficient.

Figure 10.- Concluded.

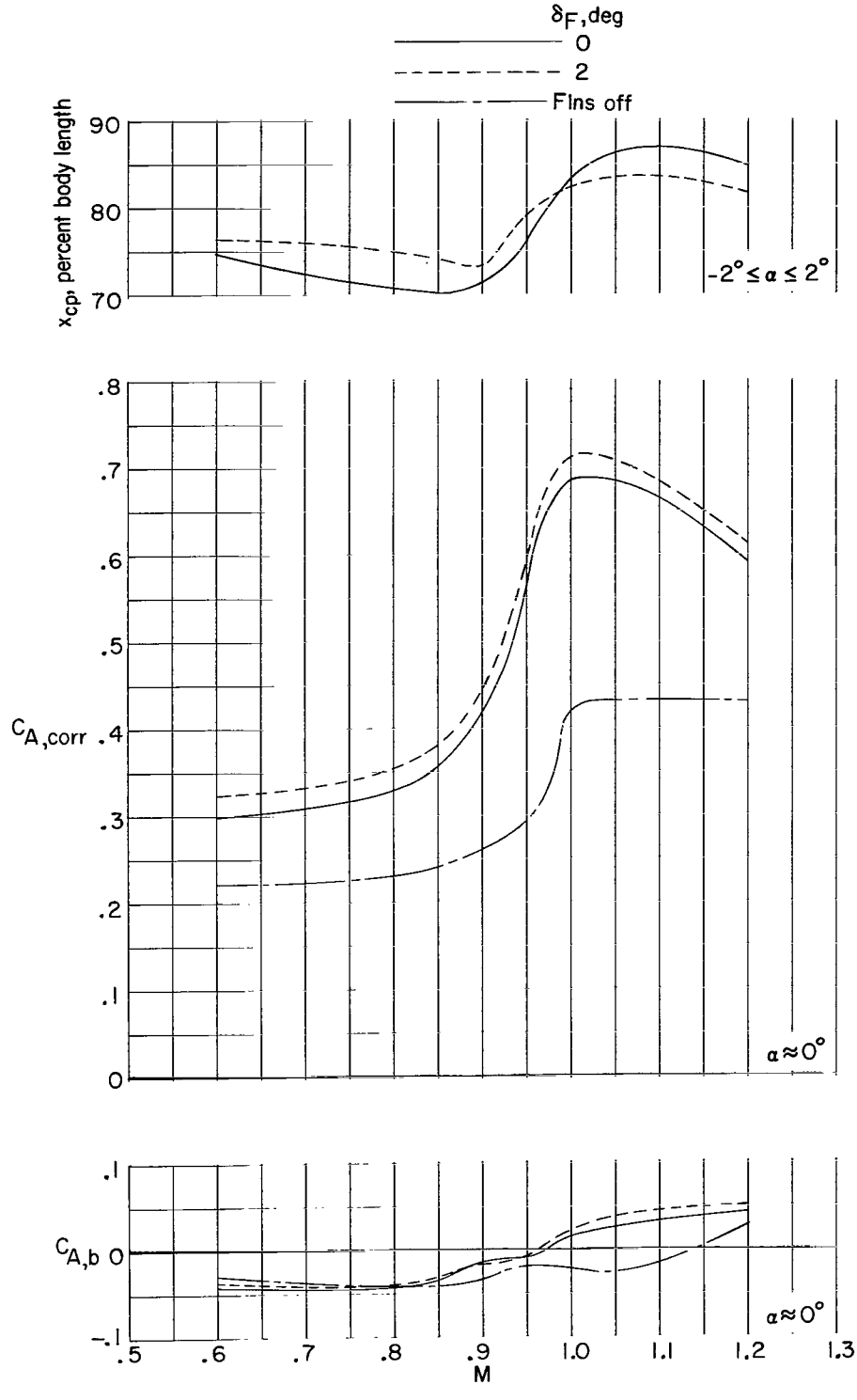

Figure 11.- Variation of center-of-pressure location, $C_{A,corr}$, and $C_{A,b}$ with Mach number. Short model; $\Phi = 0^0$.

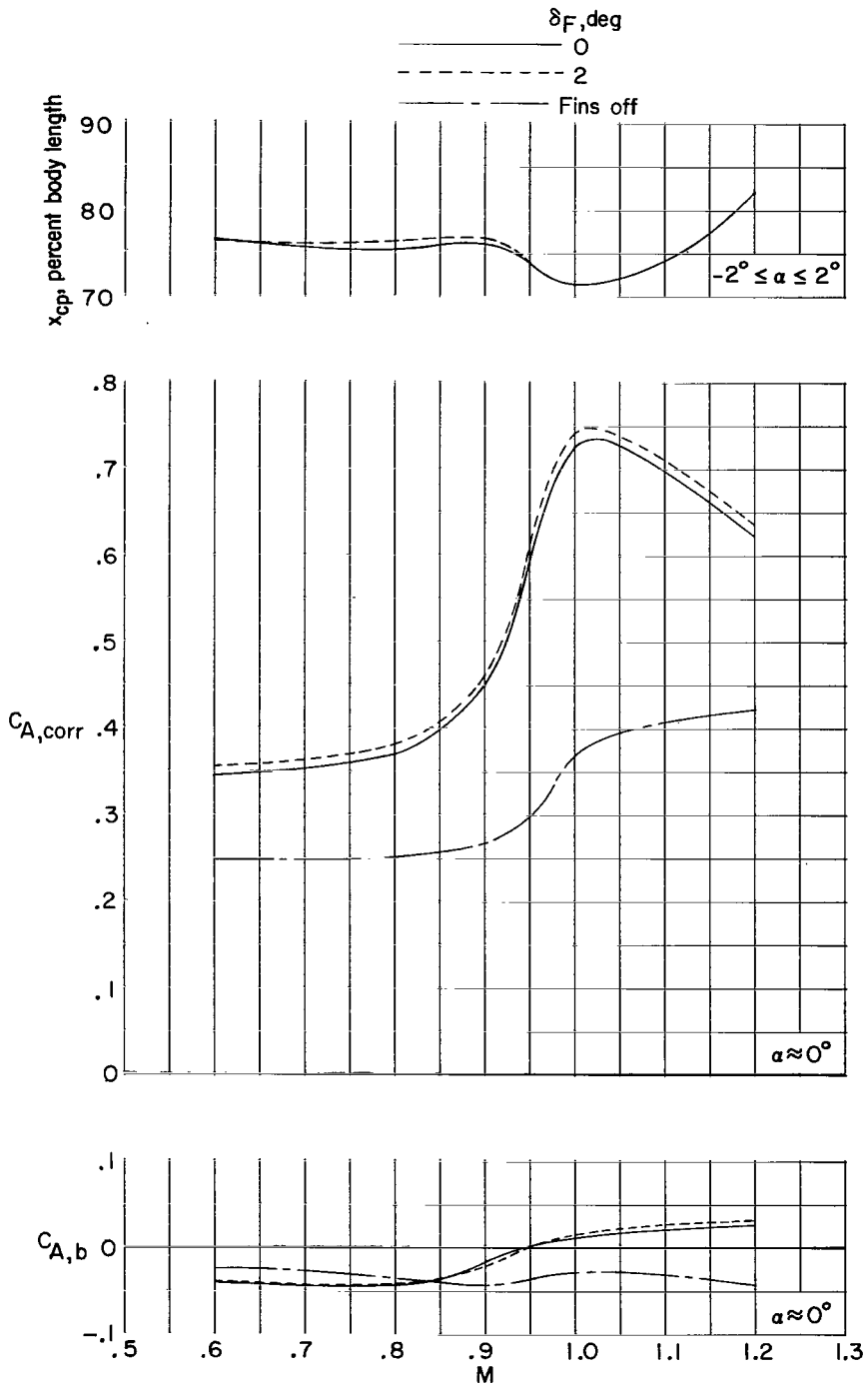

Figure 12.- Variation of center-of-pressure location, $C_{A,corr}$, and $C_{A,b}$ with Mach number. Long model; $\Phi = 0^0$.

"The aeronautical and space activities of the United States shall be conducted so as to contribute . . . to the expansion of human knowledge of phenomena in the atmosphere and space. The Administration shall provide for the widest practicable and appropriate dissemination of information concerning its activities and the results thereof."

—NATIONAL AERONAUTICS AND SPACE ACT OF 1958

NASA SCIENTIFIC AND TECHNICAL PUBLICATIONS

TECHNICAL REPORTS: Scientific and technical information considered important, complete, and a lasting contribution to existing knowledge.

TECHNICAL NOTES: Information less broad in scope but nevertheless of importance as a contribution to existing knowledge.

TECHNICAL MEMORANDUMS: Information receiving limited distribution because of preliminary data, security classification, or other reasons.

CONTRACTOR REPORTS: Scientific and technical information generated under a NASA contract or grant and considered an important contribution to existing knowledge.

TECHNICAL TRANSLATIONS: Information published in a foreign language considered to merit NASA distribution in English.

SPECIAL PUBLICATIONS: Information derived from or of value to NASA activities. Publications include conference proceedings, monographs, data compilations, handbooks, sourcebooks, and special bibliographies.

TECHNOLOGY UTILIZATION PUBLICATIONS: Information on technology used by NASA that may be of particular interest in commercial and other non-aerospace applications. Publications include Tech Briefs, Technology Utilization Reports and Notes, and Technology Surveys.

Details on the availability of these publications may be obtained from:

SCIENTIFIC AND TECHNICAL INFORMATION DIVISION

NATIONAL AERONAUTICS AND SPACE ADMINISTRATION

Washington, D.C. 20546